Title
Future Changes in Atlantic Tropical Cyclone Precipitation and Size in Convection-Permitting Regional Model Simulations

Journal
Journal of Geophysical Research: Atmospheres, 130(16)

ISSN
2169-897X

Authors
Forbis, Dakota C
Patricola, Christina M

Publication Date
2025-08-28

DOI
10.1029/2025jd043428

AGU ADVANCING EARTH AND SPACE SCIENCES

JGR Atmospheres

RESEARCH ARTICLE
10.1029/2025JD043428

Special Collection:
Climate and weather extremes in a warming climate: Processes, Prediction and Projection

Key Points:

- Future storm-total precipitation increases by 9%–48% in convection-permitting pseudo-global warming simulations of 10 tropical cyclones
- Future tropical cyclone (TC) precipitation increased at super Clausius-Clapeyron (CC) rates of 9%–17% K^{-1} for nine of the 10 TCs
- Super-CC precipitation scaling was supported by increased ascent, with minimal contributions from precipitable water and TC size

Correspondence to:
D. C. Forbis and C. M. Patricola,
dforbis@iastate.edu;
cmp28@iastate.edu

Citation:
Forbis, D. C., & Patricola, C. M. (2025). Future changes in Atlantic tropical cyclone precipitation and size in convection-permitting regional model simulations. *Journal of Geophysical Research: Atmospheres*, *130*, e2025JD043428. https://doi.org/10.1029/2025JD043428

Received 21 JAN 2025
Accepted 14 JUL 2025

Author Contributions:
Conceptualization: Dakota C. Forbis, Christina M. Patricola
Data curation: Dakota C. Forbis
Formal analysis: Dakota C. Forbis
Funding acquisition: Christina M. Patricola
Investigation: Dakota C. Forbis
Methodology: Dakota C. Forbis, Christina M. Patricola
Project administration: Christina M. Patricola

Future Changes in Atlantic Tropical Cyclone Precipitation and Size in Convection-Permitting Regional Model Simulations

Dakota C. Forbis[1] and **Christina M. Patricola**[1,2]

[1]Department of the Earth, Atmosphere, and Climate, Iowa State University, Ames, IA, USA, [2]Climate and Ecosystem Sciences Division, Lawrence Berkeley National Laboratory, Berkeley, CA, USA

Abstract Tropical cyclone (TC) precipitation is projected to increase in the future, although the magnitude and whether its scaling with temperature will exceed the theoretical Clausius-Clapeyron (CC) rate remains uncertain. In this study, we investigated future changes in TC precipitation and its scaling with temperature in 10 TC events that impacted the United States and Caribbean Islands. We performed four-member ensembles of convection-permitting regional model simulations for each TC under historical conditions and under a high-emissions scenario for the mid-21st century. We found that future TC precipitation in a reference frame following the TC increased up to ~1.5 times the historical for all 10 TCs and scaled at super-CC rates of 9%–17% K^{-1} for nine of the 10 TCs. Precipitable water scaling was less than precipitation scaling for nine of 10 TCs, indicating that it alone did not fully explain the future TC precipitation changes. Midtropospheric ascent increased in the future by 8%–30% for nine of the 10 TCs and supported the super-CC precipitation increases. For TC size, we found that the radius of maximum wind during peak TC intensity decreased for nine of 10 TCs by up to 40%; however, the correlation with precipitation scaling was weak and insignificant. In addition, we found that thermodynamically driven TC translation speed exhibited no systematic future change and poorly explained regional storm-total precipitation changes. This study indicates that TCs can enhance future flooding risk regardless of changes in TC size or translation speed, with precipitation increases that exceed simple theoretical thermodynamic estimates.

Plain Language Summary Tropical cyclone (TC) precipitation is projected to increase in the future, although the magnitude and how it will compare to theoretical estimates based on thermodynamics remains uncertain. In this study, we investigated future changes in TC precipitation in 10 TC events that impacted the United States and Caribbean Islands. We performed high-resolution numerical model simulations for each TC under historical conditions and under a high greenhouse gas emissions scenario for the mid-21st century. We found that future TC precipitation increased up to ~1.5 times the historical for all 10 TCs and exceeded the theoretical estimate for nine of the 10 TCs. Increases in midtropospheric ascent supported the precipitation increases beyond the theoretical estimates, while changes in atmospheric moisture and TC size did not.

1. Introduction

Tropical cyclones (TCs) have resulted in nearly 6,900 fatalities and cost ~\$1.4 trillion in the United States between 1980 and 2023 (National Ocean and Atmospheric Administration (NOAA)/National Centers for Environmental Information 2024). Precipitation from TCs accounted for 27%–57% of TC-related fatalities depending on the time period (1963–2012 and 2013–2022; Brennan et al., 2023; Rappaport, 2014). TC impacts are projected to increase in the future due to a combination of population increase and changing TC characteristics. The population vulnerable to TC damage in the United States is projected to increase from ~1.2 million to ~10 million by 2075 (Dinan, 2017), while future increases in TC winds and precipitation (Carroll-Smith et al., 2021; Knutson et al., 2013, 2015; Patricola & Wehner, 2018) may enhance TC impacts. The combination of increasing coastal development and climate change is projected to increase landfalling TC costs in the United States by \$123 billion in 2075, relative to 2015 costs (Dinan, 2017), while global TC costs may increase by \$53 billion per year by the end of the 21st century (Mendelsohn et al., 2012). The impacts of TC precipitation may worsen under climate change as TC precipitation is anticipated to become the greatest contributor to Gulf Coast flooding in a future climate (Gori et al., 2022), while flooding from storm surge is also expected to worsen due to sea-level rise (Tebaldi et al., 2012).

Resources: Dakota C. Forbis, Christina M. Patricola
Software: Dakota C. Forbis, Christina M. Patricola
Supervision: Christina M. Patricola
Validation: Dakota C. Forbis
Visualization: Dakota C. Forbis
Writing – original draft: Dakota C. Forbis, Christina M. Patricola
Writing – review & editing: Christina M. Patricola

There has been growing evidence for small increases in TC precipitation during the recent historical period. Climate change since the preindustrial period led to a 4%–9% increase in TC precipitation based on convection-permitting simulations of three TC events that occurred in the 21st century (Patricola & Wehner, 2018). Similarly, TC precipitation during the 2020 Atlantic hurricane season was enhanced by climate change by 5% and 8% for tropical storms and hurricanes, respectively, based on preindustrial and historical climate simulations (Reed et al., 2022). Furthermore, TC precipitation observations from 1900 to 2017 revealed that the risk for heavy precipitation from hurricanes and previously hurricane-strength tropical storms has increased throughout the past several decades (Touma et al., 2019).

In addition to evidence that climate change has already impacted TC precipitation in the modern era, there is consensus that TC precipitation will increase in the future due to climate change, although the magnitude of the increase remains uncertain. Convection-permitting regional climate model simulations of nine historical Atlantic TC events projected increases in TC precipitation of 14%–37% at the end of the 21st century under a high greenhouse gas emissions scenario (Patricola & Wehner, 2018). Similar experiments for TCs analogous to Hurricane Ivan (2004) under three high-emissions climates showed that future TC precipitation may be enhanced by 66%–101% (Carroll-Smith et al., 2021). Under a moderate emissions scenario, late 21st century global climate experiments projected precipitation increases of 11%–30% for hurricane-strength TCs (Knutson et al., 2015). Idealized global climate model experiments with 2 K of sea-surface temperature (SST) warming and doubled CO_2 concentrations projected that TC precipitation may increase by 10%–20% (Scoccimarro et al., 2014; Villarini et al., 2014). In addition to projections for overall TC precipitation increases, precipitation from the TC inner core may increase the most in a future climate (Knutson et al., 2015; Patricola & Wehner, 2018). Future TC precipitation increases in the inner core are driven by increased greenhouse gas concentrations, whereas the atmospheric effect of future decreases in aerosols works to decrease TC precipitation in the inner core and increase it in the outer bands, based on climate model experiments (Sena et al., 2024).

The theoretical Clausius-Clapeyron (CC) relationship, which estimates that water vapor in a saturated atmosphere increases by ~7% K^{-1} of warming, is often used as a "back-of-the-envelope" estimate for potential precipitation changes (Trenberth et al., 2003), although there are many reasons why precipitation changes may deviate from the CC rate. Tropical cyclone precipitation may scale with CC based on comparisons between historical and pre-industrial climate experiments (Reed et al., 2020), although coarse-resolution climate simulations show that TC precipitation scaling in the future may be lower than CC at ~5% K^{-1} (Stansfield & Reed, 2023). However, there is evidence that TC precipitation within 100 km of the TC center may exhibit super-CC scaling in a future climate because of increased low-level moisture convergence (Liu et al., 2019). TC precipitation in a reference frame following the TC is influenced by thermodynamic factors, including atmospheric water vapor, which scales at the CC rate if relative humidity (RH) remains constant and dynamical factors including updrafts and low-level convergence (Dougherty & Rasmussen, 2021; Lenderink et al., 2017). Furthermore, TC precipitation can be related to TC intensity (Matyas, 2010; Touma et al., 2019) and TC size (Konrad et al., 2002). TC size may increase with RH based on an idealized study (Hill & Lackmann, 2009), although others found that TC size may be insensitive to RH (Frisius, 2015) and that TC size is sensitive to the model used (Schenkel et al., 2023). Tropical cyclone size is projected to grow in global climate model simulations under doubled CO_2 concentrations (Kim et al., 2014). Finally, observed TC precipitation rates depend on TC translation speed, with fast-moving TCs producing TC precipitation rates 24% greater than slow-moving TCs due to enhanced inflow and vertical wind shear (Tu et al., 2022).

Regional accumulated TC precipitation in a reference frame fixed on a given geographic location is also related to TC translation speed. Slow-moving TCs can enhance the probability for heavy precipitation falling over areas ~2,500 km^2 (Konrad et al., 2002), as was the case for Hurricane Harvey (Risser & Wehner, 2017). A 16% slowdown in Atlantic TC translation speed has been observed for TCs that made landfall between 1949 and 2016 (Kossin, 2018). However, future changes in TC translation speed remain uncertain, as there is potential for an increase in the frequency of fast-moving TCs in the midlatitudes and a decrease in the frequency of slower-moving TCs at lower latitudes in the future based on ensembles of climate model simulations (Yamaguchi et al., 2020).

Uncertainty remains regarding the magnitude of future TC precipitation projections, which is an important problem given the growth of populations vulnerable to TC impacts. In this study, we investigate the questions: (a) How does historical TC precipitation change under mid-21st century thermodynamic environments? and (b) How

Table 1
List of Tropical Cyclones (TCs) Included in This Study With the Observed First Landfall Dates for the United States and Its Territories and the Dates for the Model Initial Condition and the End of Analyses for Each TC

Hurricane name and year	Date of landfall in the U.S. or territories	Date for initial condition (HHMM YY-MM-DD)	Date for end of analyses (HHMM YY-MM-DD)
Bob (1991)	1720 UTC 1991-08-19	0600 UTC 1991-08-18	1500 UTC 1991-08-20
Florence (2018)	1115 UTC 2018-09-14	0000 UTC 2018-09-13	1200 UTC 2018-09-17
Harvey (2017)	0300 UTC 2017-08-26	0000 UTC 2017-08-25	1500 UTC 2017-08-31
Ian (2022)	0200 UTC 2022-09-28	0600 UTC 2022-09-27	0600 UTC 2022-09-30
Ivan (2004)	0650 UTC 2004-09-16	1800 UTC 2004-09-14	0000 UTC 2004-09-20
Katrina (2005)	1110 UTC 2005-08-29	0000 UTC 2005-08-28	0600 UTC 2005-08-31
Maria (2017)	1015 UTC 2017-09-20	1200 UTC 2017-09-18	0300 UTC 2017-09-21
Matthew (2016)	1500 UTC 2016-10-08	1200 UTC 2016-10-06	0000 UTC 2016-10-10
Rita (2005)	0740 UTC 2005-09-24	1800 UTC 2005-09-22	0600 UTC 2005-09-26
Sandy (2012)	2330 UTC 2012-10-29	1200 UTC 2012-10-28	0600 UTC 2012-10-31

does future TC precipitation scaling with SSTs compare to the CC rate, and what are the physical mechanisms behind any deviations from CC? To address these questions, we simulated 10 landfalling Atlantic TCs, representing historically impactful events across a range of intensity and geography, in the historical and a future climate. Our research helps advance understanding on this topic, as we focused on multiple TC events, used a convection-permitting model to reduce uncertainty associated with convective parameterization, and investigated changes in TC precipitation as they may relate to changes in precipitable water, TC dynamics, and TC translation speed.

2. Data

2.1. Tropical Cyclone Cases

We selected 10 Atlantic TCs, including the four TCs analyzed in Forbis et al. (2024). The cases included TCs from the satellite era that attained hurricane status and made landfall in the United States or Puerto Rico (Table 1). We chose these 10 TCs as they were impactful, represented a wide range of TC intensities, and impacted different geographic locations.

2.2. Observations and Reanalysis Products

Observations for TC locations, maximum 10-m wind speeds, and minimum sea-level pressure were obtained from the Atlantic Hurricane Database (HURDAT2; Landsea & Franklin, 2013). These data were used to confirm that the simulated TCs were analogous to their observed counterparts. Reanalysis data used for initial and lateral boundary conditions were from the hourly, 0.25° resolution, 38-level ERA5 reanalysis from the European Centre for Medium-range Weather Forecasts (ECMWF, 2017; Hersbach et al., 2020).

We obtained data from the U.S. Department of Energy (DOE) Energy Exascale Earth System Model (E3SM) v1.1 for the "historical" experiment for 1980–2014 and "SSP585" experiment for 2040–2060 (Bader et al., 2019, 2020), with the latter representing the Shared Socioeconomic Pathways SSP5-8.5 emissions scenario (Meinshausen et al., 2020). We used data for air temperature, surface temperature, SSTs, surface pressure, sea-level pressure, RH, and geopotential height. We also obtained projected future concentrations for seven greenhouse gases under the SSP5-8.5 scenario for 2050, including CO_2, CH_4, N_2O, three chlorofluorocarbons, and CCl_4 (Meinshausen et al., 2020).

To compare simulated precipitation to observed, we used hourly National Centers for Environmental Prediction/Environmental Modeling Center's (NCEP/EMC) 4-km Gridded Data Stage IV Data (Du, 2011), satellite observations from the National Aeronautics and Space Administration's ∼10-km half-hourly Integrated Multi-Satellite Retrievals for Global Precipitation Measurement (IMERG; Huffman et al., 2020), and 24-hr analyses from the ∼4 km gridMET data set (Abatzoglou, 2013). We used three data sets as the Gridded Data Stage IV Data

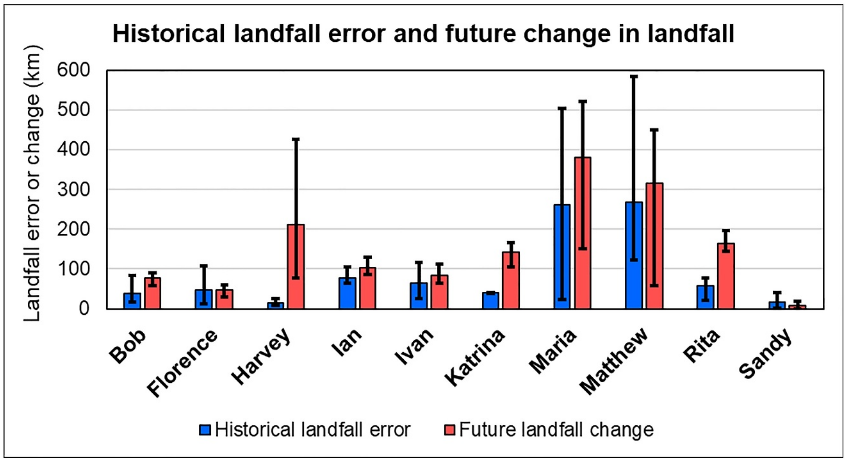

Figure 1. Ensemble-mean landfall error (distance between historical tropical cyclone (TC) landfall points and observed TC landfall point, blue) and future change in landfall (distance between future TC landfall points and historical TC landfall points, red) for Hurricanes Bob through Sandy. Error bars indicate the ensemble spread.

contained data for all TCs with the exception of Hurricanes Bob and Maria, which were included in the gridMET data set and IMERG data set, respectively. We included IMERG as it was the only data set to cover the Greater Antilles for Maria and included precipitation over ocean. Including multiple data sets also allowed us to evaluate the uncertainty in the observations. The NCEP/EMC data set likely has the least uncertainty given that it is based on radar estimates that have been corrected with rain gauge data. The gridMET is based on a combination of gridded climate data and reanalysis data and would likely have more uncertainty than NCEP/EMC. IMERG may have the most uncertainty, as it is derived from satellite observations.

3. Convection-Permitting Regional Climate Model Simulations

We used the Weather Research and Forecasting model v4.3.0 (Skamarock et al., 2021) for consistency with Forbis et al. (2024). Simulations used a convection-permitting resolution of 4 km with 50 vertical levels. Parameterizations were unchanged from Forbis et al. (2024), including the Mellor-Yamada-Janjić planetary boundary layer scheme (Janjić, 1994), Thompson microphysics scheme (Thompson et al., 2008), Noah land-surface model (Chen & Dudhia, 2001), and Rapid Radiative Transfer Model scheme (Iacono et al., 2008). We used the stochastic kinetic energy backscatter scheme (Berner et al., 2011; Duda et al., 2016; Shutts, 2005) to perform four-member ensembles for each TC in the historical and future climate.

We initialized each simulation ∼36 hr prior to the TC's first landfall (except for Katrina which was initialized ∼36 hr prior to its second landfall) over the contiguous United States or Puerto Rico for ample spin-up time (Table 1). We used data from 12 hr after initialization to the endpoint of each TC's analysis period (Table 1), which was determined by the timing of TC dissipation.

3.1. Future Climate Experiments

To represent TCs in a mid-21st century climate, we used the pseudo-global warming method (Patricola & Wehner, 2018; Schär et al., 1996). This method uses synoptic conditions analogous to the historical climate, with a future climate perturbation to represent a given weather event if a similar event occurred in a future climate. This requires calculating the difference ("delta") between a projected future climate and the historical climate conditions and adding the deltas to the initial condition and lateral boundary conditions from reanalysis. For example, the TC-following future SST change is shown in Figure 11b. As in Forbis et al. (2024), we used the E3SM v1.1 historical simulation for 1980–2014. In particular, the historical climatologies were created using 20-year periods that include the year in which the TC occurred (1980–1999, 1990–2009, and 1995–2014 for TCs that occurred during the 1990s, the 2000s, and the 2010s through the 2020s, respectively). The 2040–2060 climatology from the SSP585 simulation was used for the future climate. The climatologies for the historical and future periods were from the particular month in which each TC occurred. We used data for the variables discussed in Section 2.2. Although aerosol concentrations decrease in the future under SSP585, we did not include aerosol perturbations in

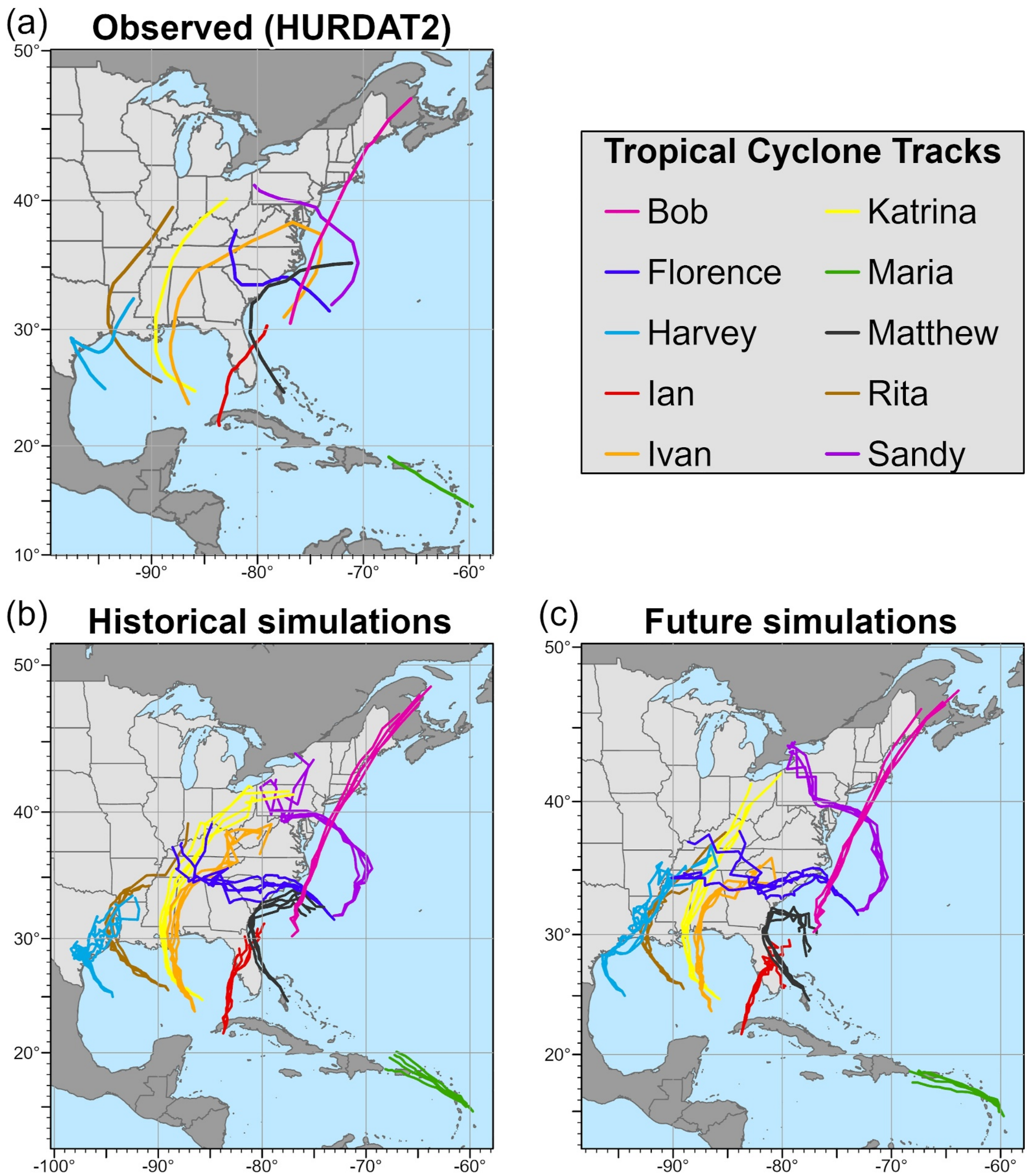

Figure 2. Tropical cyclone tracks from (a) HURDAT2 observations and the (b) historical and (c) future simulations.

our future experiments, which focused on the combined effect of ocean and atmospheric heating and greenhouse gasses on multiple TCs.

3.2. TC Tracking and TC-Following Data

We tracked the position of the simulated TCs every 3 hours based on the location of minimum sea-level pressure. To verify that the simulated TCs were representative of their real-world counterparts, we assessed simulated TC track and intensity including any errors in the simulated historical landfall, and any deviations in landfall between the future and historical simulations. Mean landfall error in the historical TC tracks was 15–268 km for all 10 TCs (Figure 1). The future TC landfalls deviated from the historical by 8–381 km. The largest deviations in landfall were for TCs like Maria, which impacted Puerto Rico and several other islands, but sometimes made landfall on other adjacent islands in the simulations. As the only landfall Maria made was on a different island in these cases, the distance is calculated using these landfall points with the corresponding historical or future ensemble

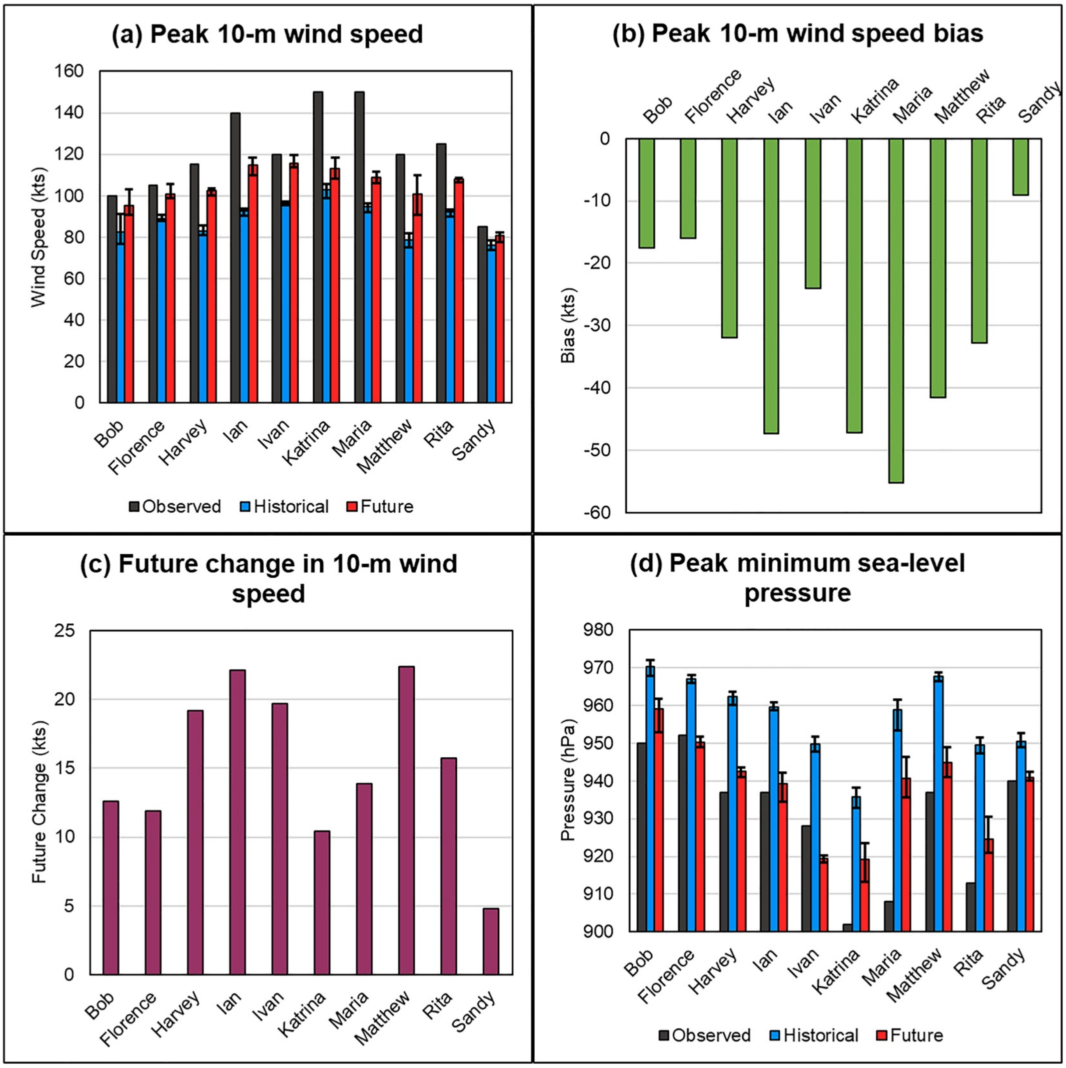

Figure 3. (a) Peak 10-m wind speed (kts) from HURDAT2 observations (black) and the ensemble-mean historical (blue) and future (red) simulations, (b) the model bias in peak 10-m wind speed (kts) from the ensemble-mean historical simulations minus HURDAT2 observations, (c) the future change in (c) peak 10-m wind speed (kts), and (d) peak minimum sea-level pressure (hPa) HURDAT2 observations (black) and the ensemble-mean historical (blue) and future (red) simulations. Future changes in peak 10-m wind speed and peak minimum sea-level pressure are statistically significant ($p < 0.05$) for all hurricanes. Error bars in (a) and (d) represent ensemble spread.

member's landfall point over Puerto Rico. Overall, historical TC tracks were relatively accurate, while the future TC tracks were comparable to those in the historical climate, despite relatively high landfall error for Maria and Matthew and large future deviations for Harvey, Maria, and Matthew (Figures 2a–2c).

We calculated the three-hourly maximum 10-m wind speed and translation speeds for each TC. For TC translation speeds, we first calculated the three-hourly translation speed between all TC locations as determined by minimum sea-level pressure for each ensemble member. For our analysis, we considered the ensemble-mean translation speed averaged from approximately 24 hr before landfall or close approach to land through the end of the analysis period.

In addition, we composited data for precipitation and environmental variables in a TC-following framework centered on the TC. In particular, we collected three-hourly precipitation rates, separated for when the TC was centered over land or over ocean, to calculate TC-following, storm-total precipitation. This was done within a 564 × 564 km box centered on the location of minimum sea-level pressure for each TC, except for Sandy which required a 1,004 × 1,004 km box since it was an unusually large storm. In addition, we composited TC-following SST, 700 hPa vertical velocity (ω), 700 hPa RH, precipitable water, and 10-m wind speed. The future change in composited SST underlying the TC was used to calculate future precipitation scaling. We analyzed vertical velocity so we could identify regions of intense convection and how their future changes might contribute to precipitation scaling that deviates from the CC rate. 10-m wind speed was used to calculate TC size based on the radius of maximum winds (RMW) and the 34-kt wind (tropical storm strength) radius (R34) at the time of peak TC-strength. As the TC wind fields were not perfectly circular, we calculated the ensemble-mean maximum extent of the 34-kt winds for all four quadrants of each TC. We also calculated the change in maximum 34-kt wind extent over all quadrants of each TC together at peak TC-strength to evaluate changes in the maximum TC-strength wind radius.

4. Results

4.1. TC Intensity and Wind Field

TCs simulated in the historical climate often did not reach their observed peak 10-m wind speed over the analysis period (Figures 3a and 3b), possibly due to the parameterization schemes used, the initial condition, model resolution, and/or the reanalysis data used. A robust future increase in TC intensity was projected for all TCs, with increases in 10-m wind speed of ∼5–22 kts or 6%–29% (Figure 3c) and decreases in the minimum sea-level pressure of ∼10–30 hPa (Figure 3d). The future ensembles produced distinctly stronger (i.e., no overlap) 10-m wind speeds (Figure 3a) and minimum sea-level pressure (Figure 3d) compared to the historical ensembles for 8 of the 10 TC cases and all 10 TC cases, respectively. This response is consistent with prior research for an end-of-century high-emissions scenario (Patricola & Wehner, 2018).

We calculated the ensemble-mean RMW and 34-kt wind radius (R34) for each TC at peak intensity as measures of TC size. R34 was calculated for each quadrant of each TC independently and used the maximum extent per quadrant from the historical and future climates for comparison as in the HURDAT2 data set (Landsea & Franklin, 2013) and in other studies (Chavas et al., 2024; Nekkali et al., 2022). There is no systematic future change in R34 by quadrant (Figures 4a–4j, 5b, and 5d). However, the region where 10-m wind speeds over the ocean intensified the most corresponded with the future extent of the RMW in nine of 10 cases, with the exception of Matthew (Figure 4). The RMW was between ∼38 and 143 km for all 10 TCs in the historical climate, decreasing to ∼30–115 km in the future (Figure 5a). RMW decreased by up to 31 km (1%–40%) for nine of ten TCs (Figure 5c), while Bob's RMW increased by 4 km (∼8%). As TC size measured by RMW decreases, TC intensity increases, which is consistent with Carrasco et al. (2014) and suggests that the radial extent and intensity of the inner-core convection could both shrink and intensify, respectively, in a future climate. The historical simulations had a positive bias in R34 compared to HURDAT2 for eight of nine TCs for which observations existed (no observations were available for Bob). R34 was between ∼252 and 902 km for the 10 TCs in the historical climate, increasing to ∼257–968 km in the future (Figure 5b). R34 increased for six of ten TCs by ∼2–12%, while shrinking by ∼1–12% in the other four cases (Figure 5d). The projections for R34 were inconclusive as there remains uncertainty in how the size of tropical storm strength wind fields will change in the future climate.

4.2. TC Precipitation

Before evaluating future projections in storm-total precipitation, we first compared the historical simulations with observations over the region that each TC impacted (Figure 6a). Ensemble-mean storm-total precipitation over land ranged between 32 and 180 mm in the historical simulations (Figure 6b). The historical simulations produced land-based storm-total precipitation within ±20% of the NCEP/EMC observations for six out of eight TCs for which the data were available (Figure 6c). The bias in storm-total precipitation over land relative to the NCEP/EMC observations exceeded ±20% for Florence (−24%) and Ian (+45%) due to changes in TC tracks. Precipitation biases in the historical simulations were similar between the NCEP/EMC observations and the gridMET product, whereas systematic differences in the observational products resulted in negative precipitation biases for all TCs with respect to the IMERG data (Figure 6c). Future storm-total precipitation area-averaged over the land regions impacted by the TCs increased by 3%–184% for all TC cases (Figure 6d). The range in future TC precipitation projections area-averaged over the land regions impacted by the TC arises mainly because we used a fixed region for this portion of the precipitation analysis, which was sensitive to small TC-track changes in cases where the land

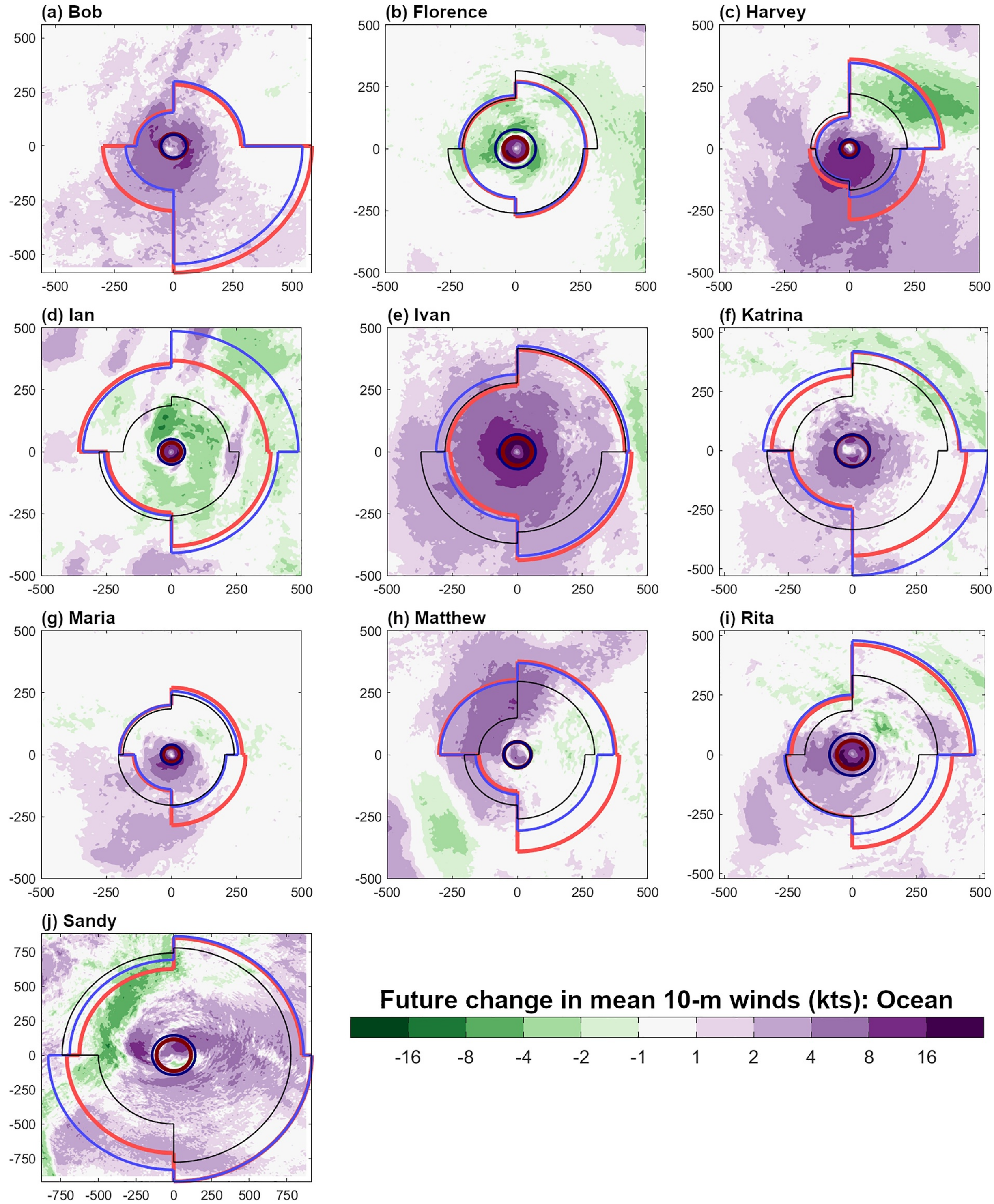

Figure 4. Tropical cyclone (TC)-following future change in 10-m wind speed (kts; shaded) averaged during times the TC center was over ocean, calculated as the ensemble-mean future minus historical simulations, for (a–j) Hurricanes Bob through Sandy. Black, bright blue, and bright red contours represent the maximum extent of the 34-kt 10-m wind speed per quadrant at peak TC intensity from observations (black), the ensemble-mean historical (blue), and future (red) simulations. Dark blue and dark red contours represent the radius of maximum winds for 10-m wind speed at peak TC intensity from the ensemble-mean historical (dark blue) and future (dark red) simulations. The x-axis and y-axis denote distances from the TC center (km).

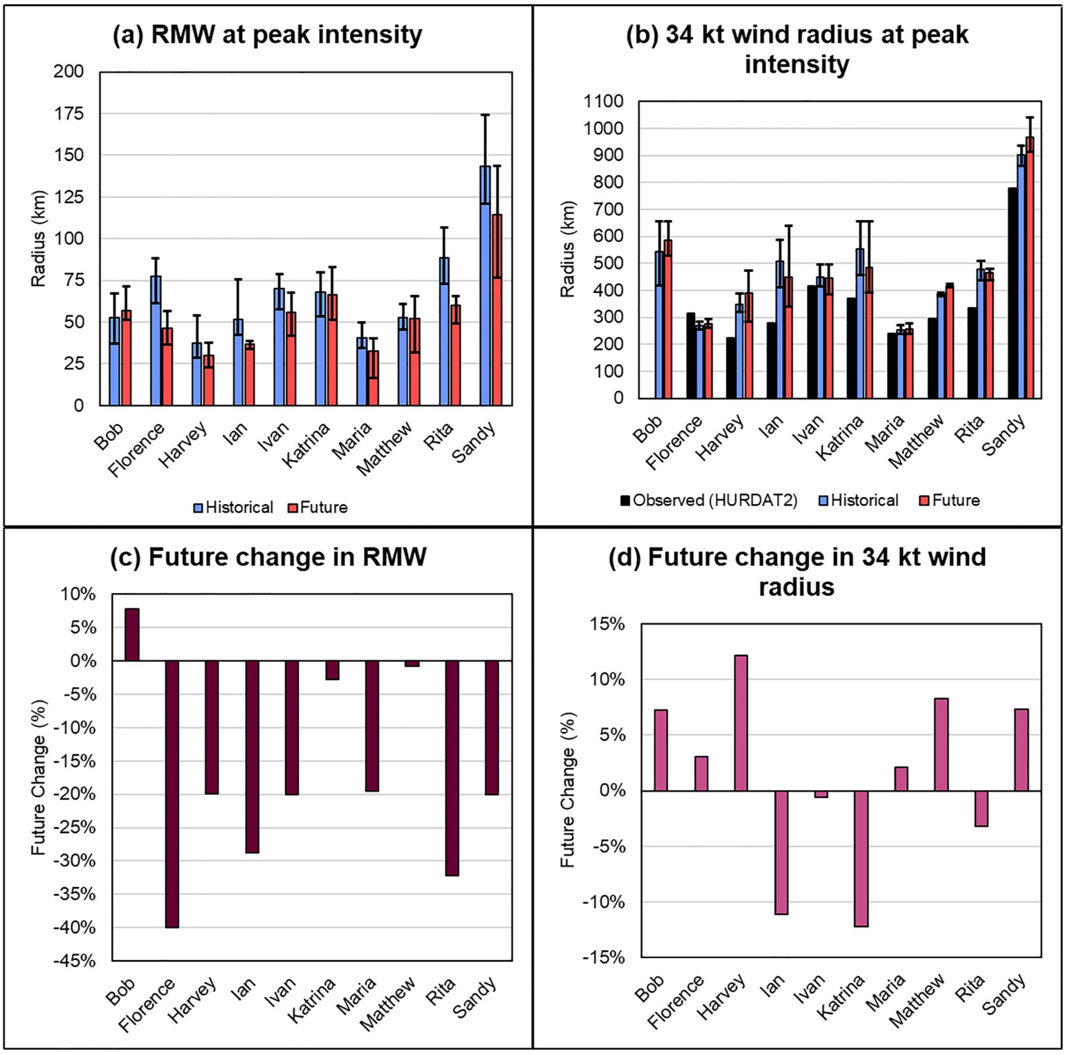

Figure 5. The ensemble-mean (a) radius of maximum winds (km) and (b) maximum 34-kt wind radius of the four quadrants (km) during peak tropical cyclone (TC) intensity for each TC from the historical (blue) and future (red) simulations. The observed maximum 34-kt wind radius from HURDAT2 is shown in (b) in black. The future change in the (c) radius of maximum winds (%) and (d) the 34-kt wind radius (%), calculated as (ensemble mean future minus ensemble mean historical)/ensemble mean historical simulations. Error bars in (a) and (b) represent ensemble spread.

region was small. For example, the land region for Hurricane Maria, which had the largest future precipitation increase, consisted of several islands, making the land-based precipitation sensitive to even small changes in TC tracks. As a result, a much larger future increase in terrestrial precipitation occurred for Maria in the fixed-region analyses due to high sensitivity to small track changes.

As our fixed-area precipitation analyses were calculated over a region and not relative to TC location, the analyses could be sensitive to small shifts in TC tracks, which can cause large fluctuations in precipitation over a particular region. We attempted to minimize this issue by making the regions large enough to capture the bulk of TC precipitation regardless of any shifts in TC tracks. However, to be certain, we also evaluated storm-total precipitation in a TC-following reference frame to account for any changes in TC tracks. This also allows us to evaluate TC precipitation over both ocean and land. Historical storm-total precipitation over land in the TC-following framework ranged between ~3 and 231 mm (Figure 7a) and increased by 14%–445% in the future simulations for eight of 10 TCs, or by 14%–60% when excluding Maria (443%) and Matthew (445%) due to high sensitivity to TC-track changes near land-ocean boundaries (Figure 7b). These increases are comparable to the fixed-region future increases in precipitation of 3%–58% for nine of ten TCs, with the notable exception of Maria

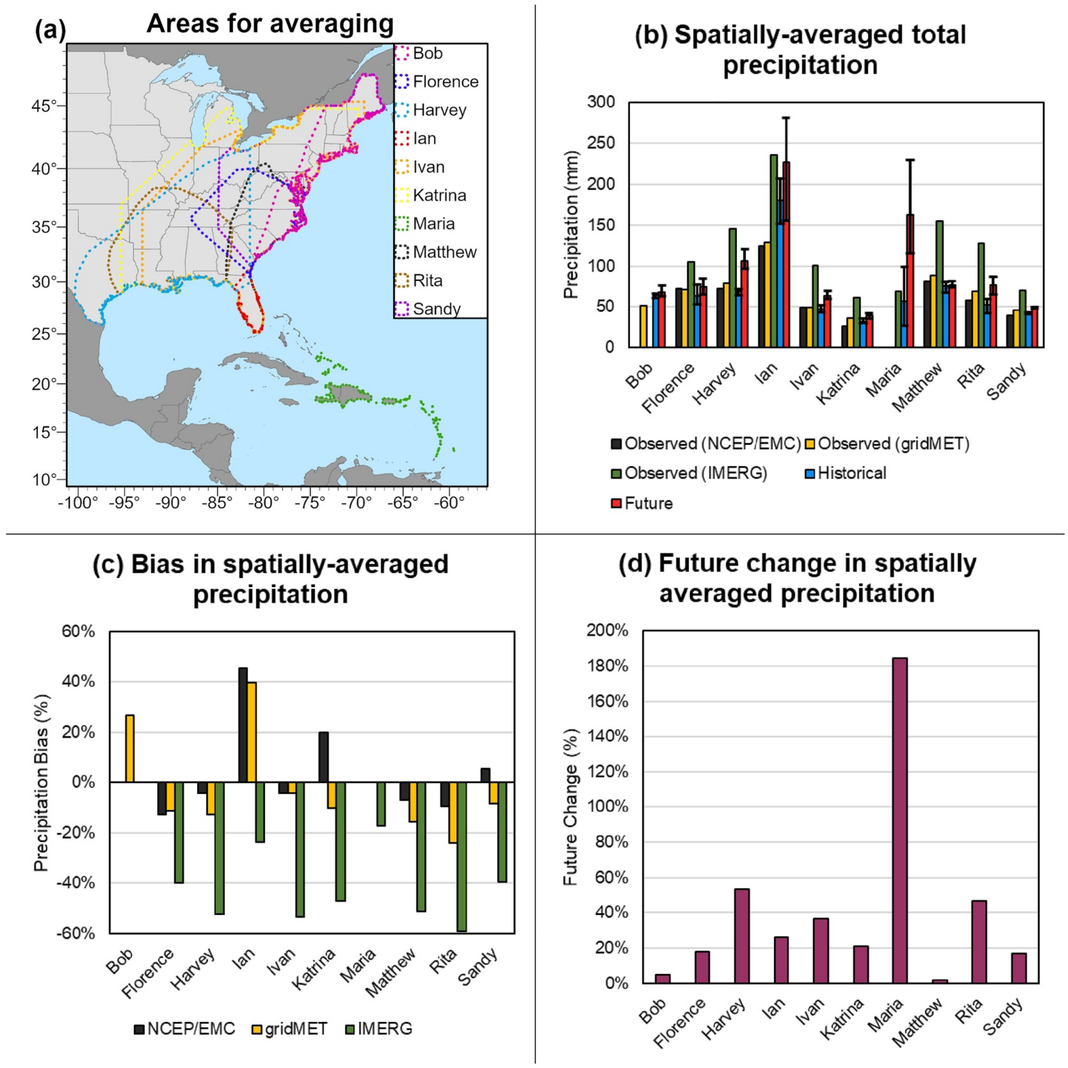

Figure 6. (a) Regions used for geographically fixed, land-based precipitation analysis for each tropical cyclone used in (b–d), (b) regionally averaged storm-total precipitation (mm) from the National Centers for Environmental Prediction (NCEP)/Environmental Modeling Center (EMC) (black), gridMET (gold), and IMERG (green) observational data sets and from the ensemble mean of the historical (blue) and future (red) simulations, with error bars representing the ensemble spread, (c) the model bias in land-based, regionally averaged storm-total precipitation (%) calculated as (ensemble-mean historical simulation minus observations)/observations based on the NCEP/EMC (black), gridMET (gold), and IMERG (green) observational data sets, and (d) the future change in land-based regionally averaged storm-total precipitation (%) calculated as the (ensemble-mean future minus ensemble-mean historical)/ensemble-mean historical simulations. Future changes in mean precipitation are statistically significant ($p < 0.10$) for all hurricanes.

which had fixed-region precipitation increases of 184%. It makes sense that there would be a high sensitivity for Hurricane Maria given the relatively small land area that it impacted. Land-based precipitation decreased by 14% and 32% for Hurricanes Bob and Harvey, respectively. TC-following storm-total precipitation over ocean also increased for eight of ten TCs by 1%–308% (1%–93% when excluding Harvey), while decreasing by 12% and 5% for Ian and Matthew, respectively (Figure 7b), due to environmental changes and TC-track changes, respectively. Overall, storm-total precipitation over land and ocean together increased by 9%–48% in the future for all TCs (Figure 7b), with all future ensemble members simulating greater storm-total precipitation than the historical ensemble members for all TCs except Ian (Figure 7a).

In addition to TC-following storm-total precipitation, we calculated TC-following three-hourly precipitation rates by averaging the three-hourly precipitation over the times in the analysis period and all ensemble members for

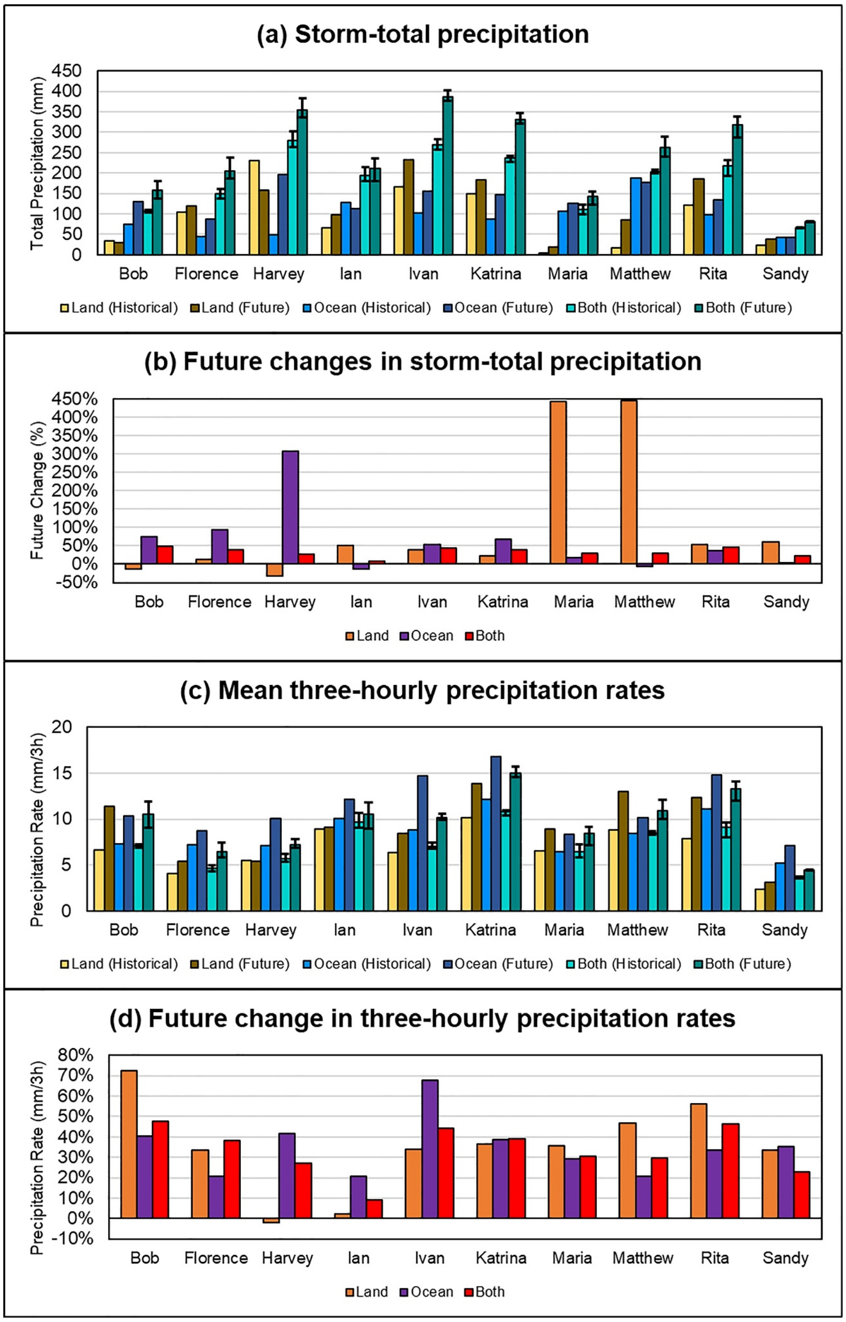

Figure 7. (a) TC-following storm-total precipitation (mm) accumulated for all times the tropical cyclone (TC) is centered over land (yellow/brown), ocean (blues), and either land or ocean (greens) from the ensemble-mean historical (lighter color) and future (darker color) simulations. (b) The future change in TC-following storm-total precipitation (%) accumulated for all times the TC is centered over land (orange), ocean (violet), and either land or ocean (red) calculated as the (ensemble-mean future minus ensemble-mean historical)/ensemble-mean historical simulations. (c) and (d) The same as (a) and (b), respectively, but for three-hourly precipitation rates (mm/3 h and %, respectively). Error bars in (a) and (c) represent ensemble spread for precipitation over land and ocean combined.

TCs when they were centered over land, ocean, and either. Considering the three-hourly precipitation rates allowed us to normalize TC precipitation with respect to TC lifetime. We discuss the spatial patterns of future precipitation changes (Figures 8 and 9), together with the quantitative changes averaged in the TC-following box. Land-based three-hourly precipitation rates did not exhibit systematic spatial patterns of future precipitation change across the 10 TC cases, with some TCs exhibiting future precipitation increases and others decreases over

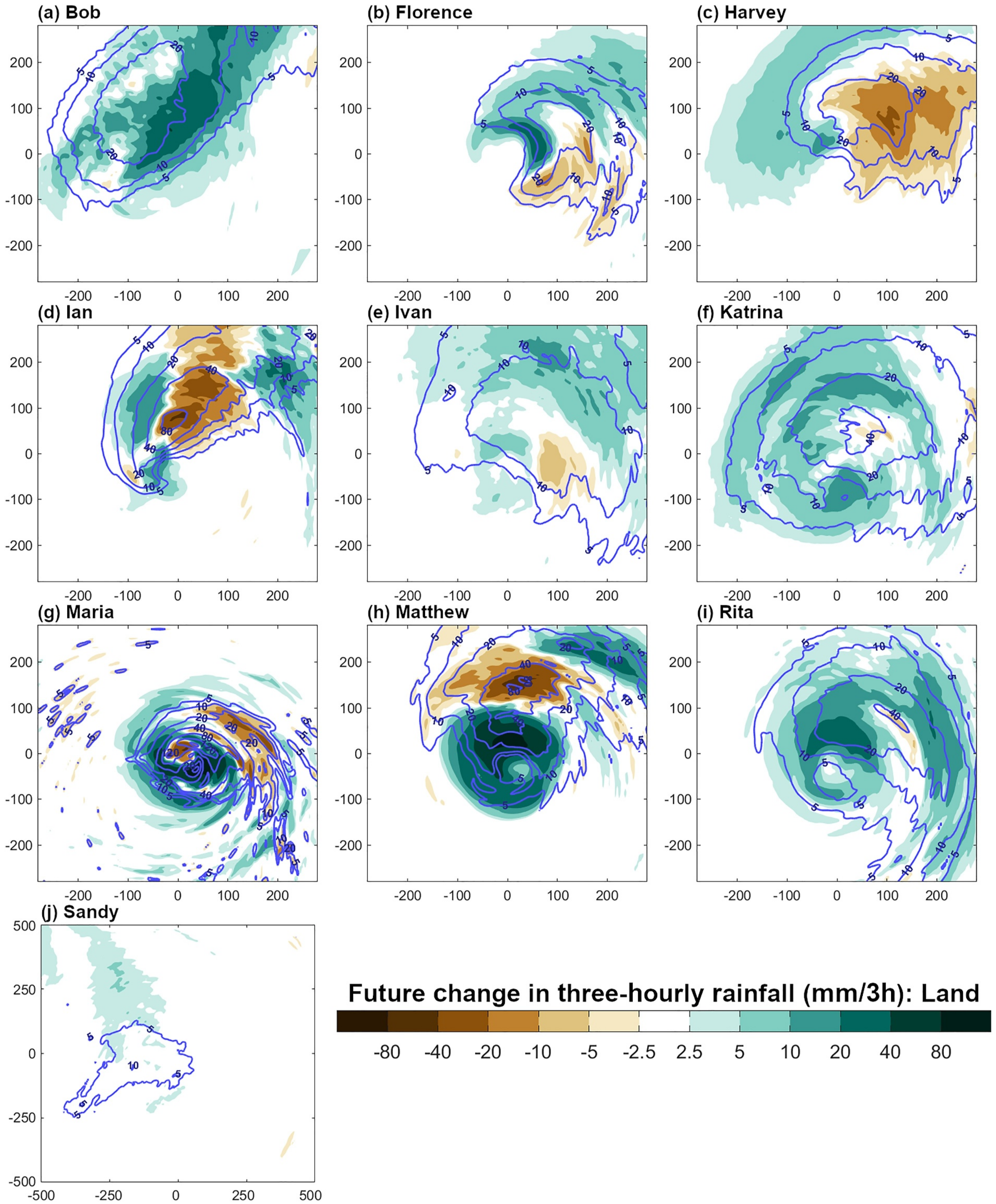

Figure 8. TC-following future change in three-hourly precipitation rates (mm/3 h; shaded) averaged during times the tropical cyclone (TC) center was over land, calculated as the ensemble-mean future minus historical simulations for (a–j) Hurricanes Bob through Sandy. Blue contours denote the ensemble-mean historical simulations' three-hourly precipitation rates (mm/3 h). The x-axis and y-axis denote distances from the TC center (km). Note that the axes cover the same spatial extent for all hurricanes except Sandy, which was an unusually large TC.

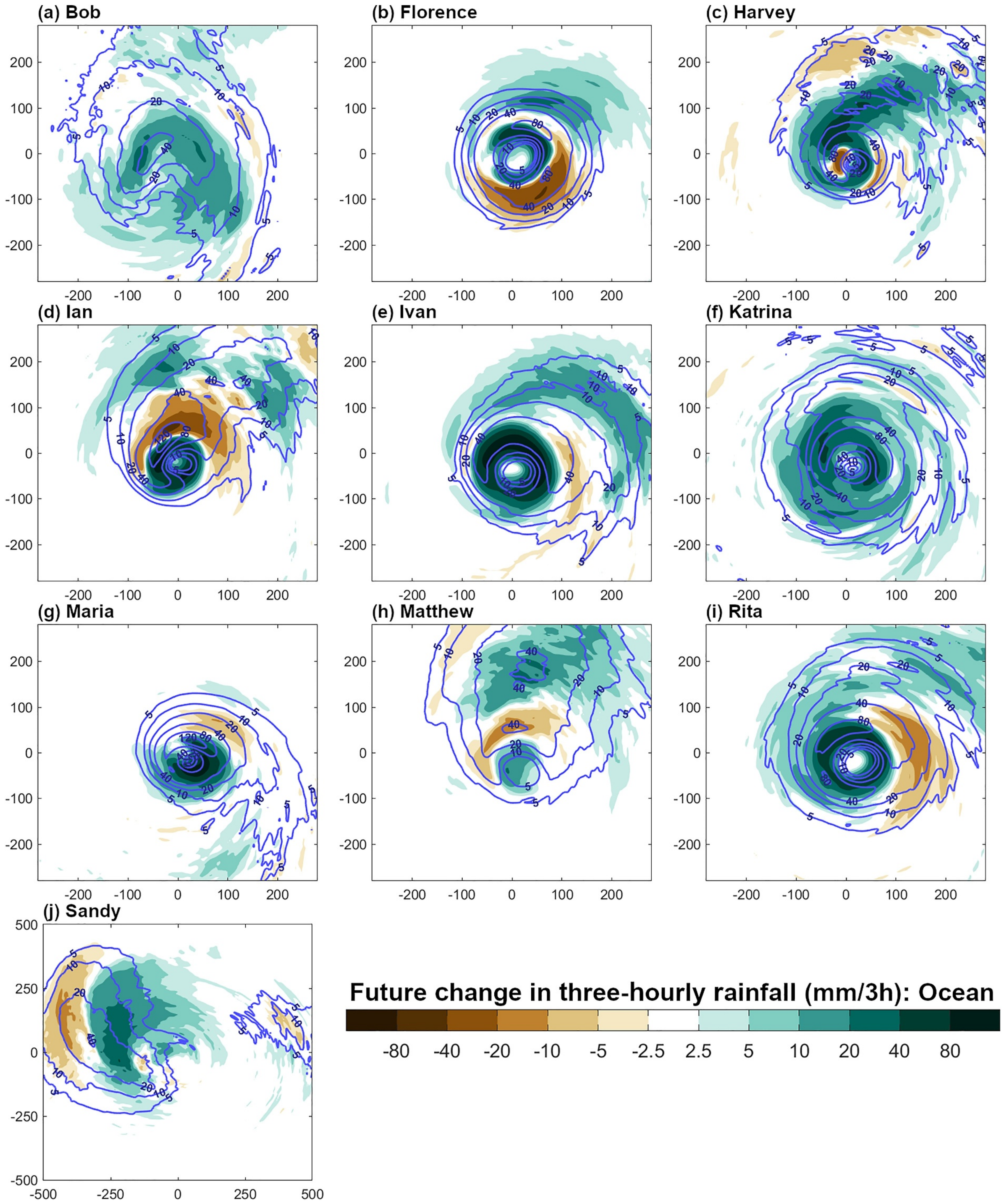

Figure 9. Same as Figure 8, but for times the tropical cyclone center was over ocean.

regions where the historical precipitation was greatest (Figure 8). However, the future precipitation changes averaged over the TC-following box were more robust across the TC cases. Historical land-based three-hourly precipitation rates in the TC-following framework ranged between 2 and 10 mm/3 hr, increasing to 3–14 mm/3 hr (2%–72%) in the future for nine of 10 TCs while decreasing for Harvey by 2% (Figures 7c and 7d).

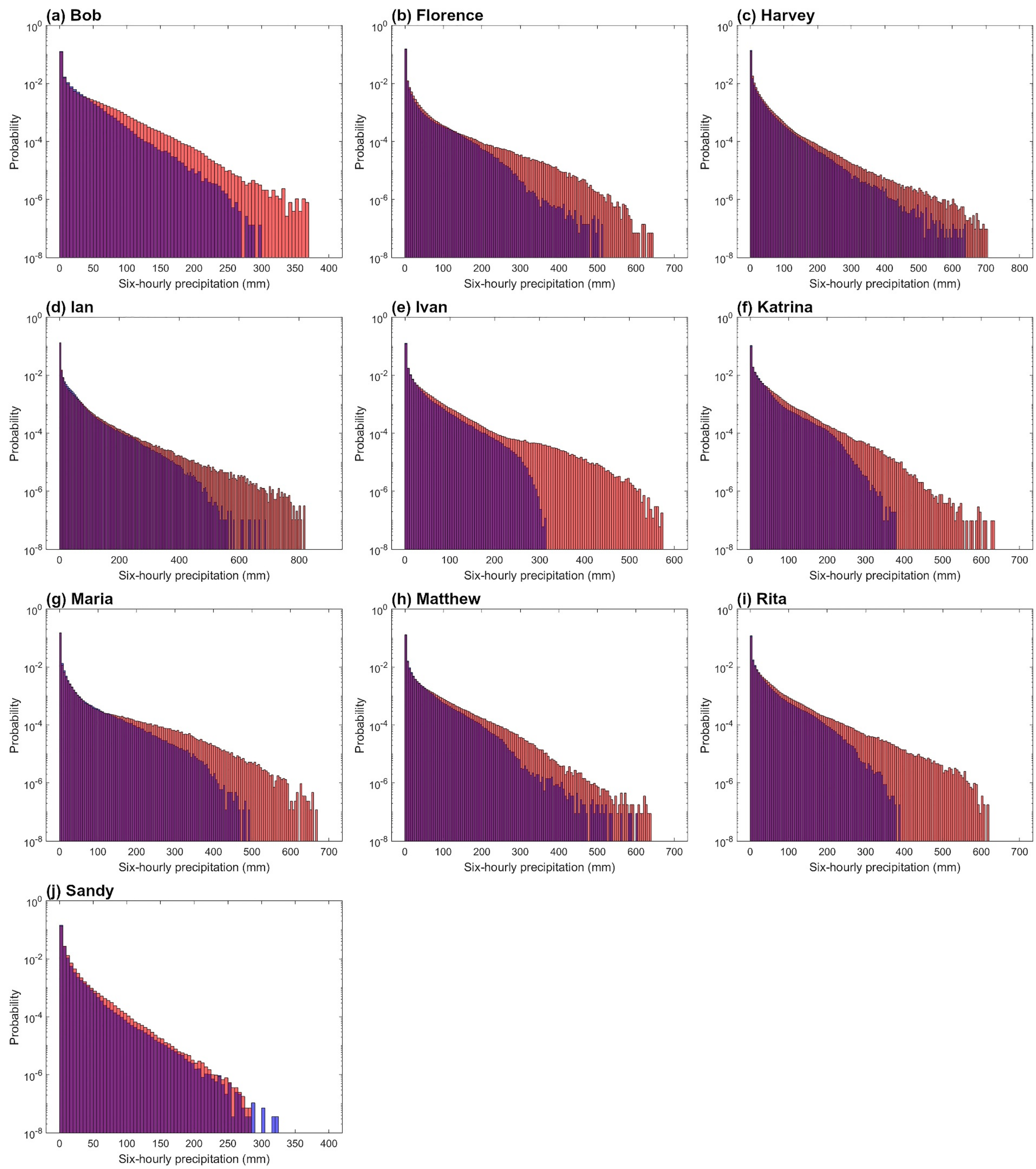

Figure 10. Probability distribution functions of six-hourly precipitation (mm) for Hurricanes Bob through Sandy (a–j). The blue denotes the historical simulations, red denotes the future simulations, and purple denotes overlap of the two simulations.

Over ocean, the regions with future increases in three-hourly precipitation rates tended to coincide with regions of the greatest historical TC precipitation rates (Figure 9). Enhancement of inner-core precipitation over ocean was projected for all TCs that had an organized inner core, with many of the TCs also exhibiting future precipitation decreases of varying magnitudes and spatial extents in the outer bands (Figure 9). The future three-hourly precipitation rates over ocean increased by a narrower range of 21%–68% for all TCs (Figure 6d). For three-hourly precipitation over both land and ocean, all TCs experienced a net increase of 9%–48% in the future (Figure 7d). We note that spatial changes in future TC precipitation were not robust across all TCs, as TC precipitation

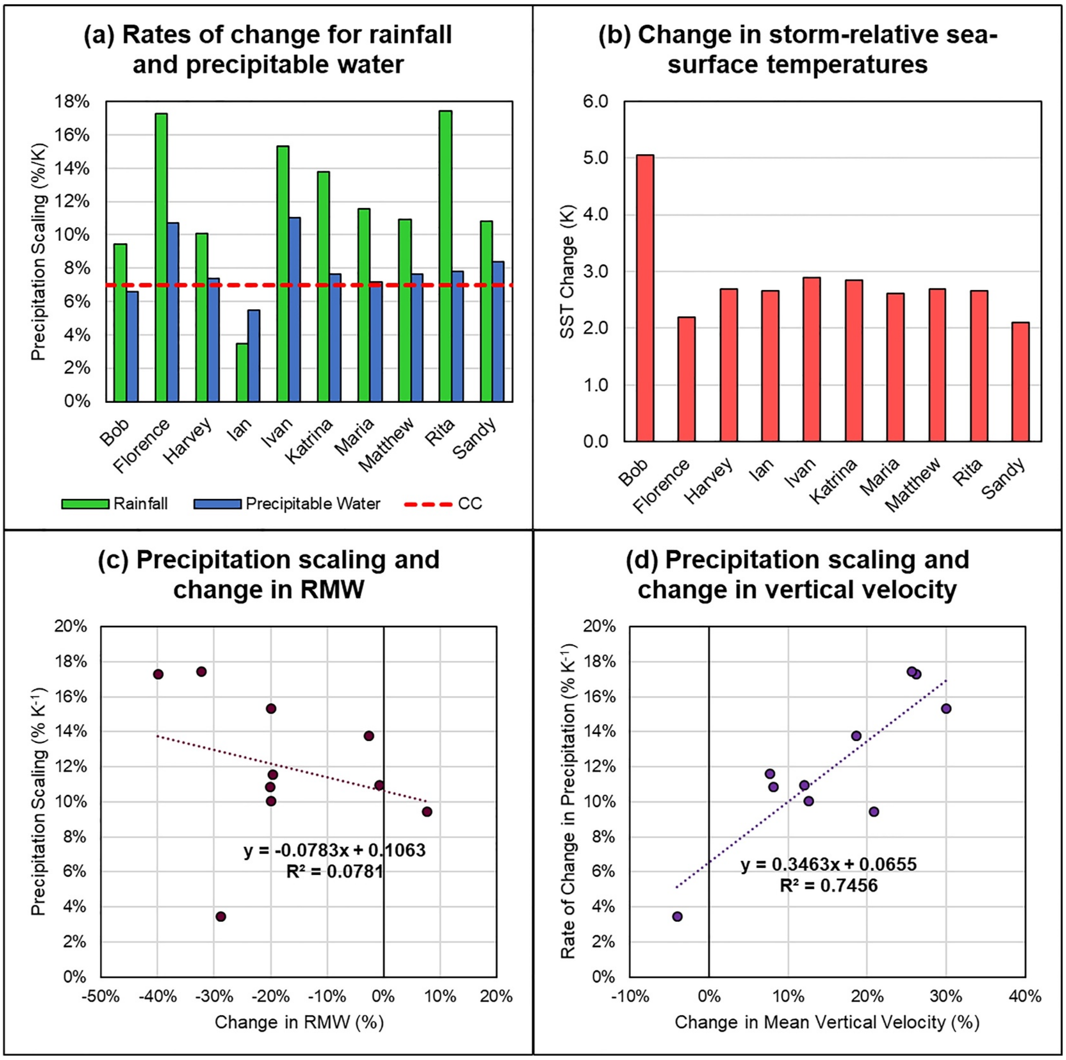

Figure 11. (a) Tropical cyclone (TC) precipitation scaling, that is, the future change in TC-following storm-total precipitation (calculated as (ensemble-mean future minus ensemble-mean historical)/ensemble-mean historical) per K of sea-surface temperature (SST) warming (% K^{-1}), for Hurricanes Bob through Sandy (green) and precipitable water scaling, that is, the future change in TC-following precipitable water per K of SST warming (% K^{-1}), for the same TCs (blue). Red dashed line represents the theoretical change in atmospheric moisture per K of SST warming (7% K^{-1}) based on the Clausius-Clapeyron relationship. (b) Future change in TC-following SSTs (K) from the future minus historical simulations for each TC. (c) Scatterplot of the relative future change in radius of maximum winds (%) on the x-axis and TC precipitation scaling (% K^{-1}) on the y-axis. Relative change calculated by (future—historical) divided by historical. The points indicate the ensemble mean for each TC, while the dashed line represents the linear trendline for the data points. (d) Same as (c), but with relative future change in 700 hPa vertical velocity ω (%) on the x-axis.

depends on both the synoptic conditions around the TC and the TC characteristics. Although a sample size of 10 TCs is large for a study like this, a larger sample size would help to better understand the common drivers for certain spatial patterns in future precipitation changes.

Finally, we investigated the distribution of six-hourly precipitation to understand changes in the probability of extremes. The probability density functions shown in Figure 10 were calculated as follows: For each TC and each climate state, six-hourly precipitation values that occurred in the TC-following box were aggregated over all grid points in the box, the entire TC analysis period, and all ensemble members. Extreme values of six-hourly precipitation are projected to occur more frequently in the future than the historical climate for all 10 TCs (Figure 10). These results are robust and consistent with both the increases in storm-total precipitation in our simulations and the future increases in the probability of extreme TC precipitation simulated by Patricola and Wehner (2018).

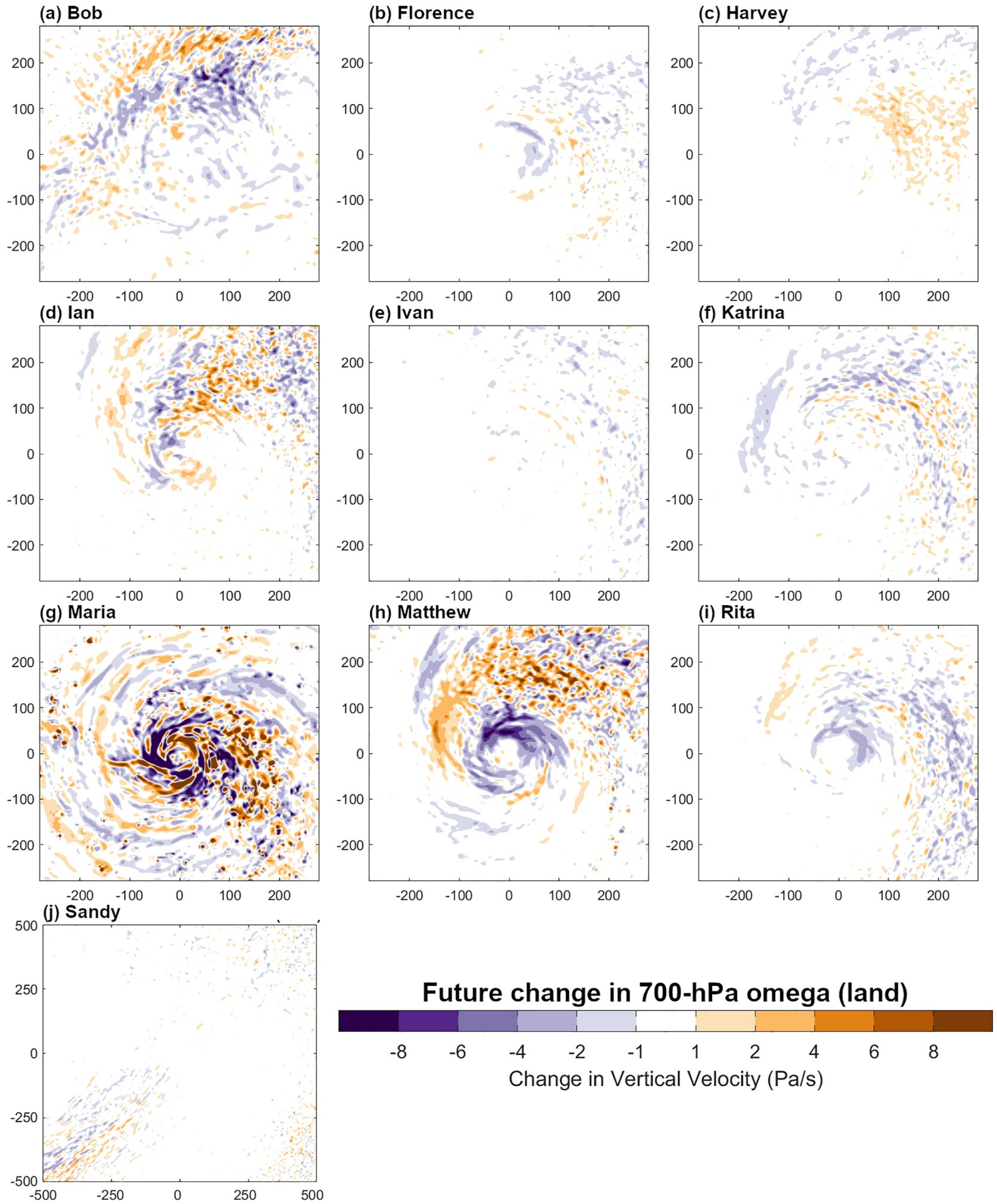

Figure 12. Future change (ensemble mean future minus ensemble mean historical) in 700 hPa ω (Pa/s; orange and violet shading) for Hurricanes Bob through Sandy (a–j) for when each tropical cyclone (TC) is centered over land. The x-axis and y-axis denote distance from the TC center (km). Note that the axes cover the same spatial extent for all hurricanes except Sandy, which was an unusually large TC.

4.3. TC Precipitation Scaling

We next analyzed the precipitation scaling (Figure 11a), calculated as the percent change in TC-following storm-total precipitation ((future minus historical)/historical) divided by SST warming in the TC-following framework (Figure 11b). This is done for comparison with the CC relationship to understand to what extent future TC precipitation changes deviated from simple thermodynamic theory. Nine of ten TCs exhibited precipitation scaling at super-CC rates, between 9% and 17% K^{-1}. Only Hurricane Ian's future precipitation increased at sub-CC rates (3% K^{-1}). In contrast, TC-following precipitable water only increased by 5%–11% K^{-1} in the future for the ten TCs, with eight of ten TCs having increases that were around or below CC, while Florence's and Ivan's precipitable water increased by ~11% K^{-1}. Our results show that not only is there potential for future TC precipitation in excess of that estimated by the CC rate but that TC precipitation may increase at rates more than double that of CC. TC precipitation rates appear to not only be able to increase at super-CC rates but to also outpace future increases in precipitable water, suggesting that changes in atmospheric moisture alone do not account for the super-CC precipitation increases. It is likely that TC dynamics are involved, specifically with respect to enhanced inner-core convection. TCs may become more efficient producers of precipitation given that the rate of precipitation enhancement is greater than the rate of precipitable water enhancement. This may be due partially to enhanced environmental heating near the surface (Stansfield & Reed, 2021) and evaporation in areas of the outer core with suppressed convection, allowing for enhanced moisture transport and instability downwind toward the inner core.

Given that TC dynamics were likely involved in the super-CC enhancement of precipitation, we analyzed the relationships between environmental variables and precipitation scaling for all TCs. To assess these relationships, we calculated the linear correlation coefficient between precipitation scaling and the future change in ensemble mean RMW and between precipitation scaling and the future change in ensemble mean 700 hPa ω, and checked whether the data exhibited a linear relationship (Figures 11c and 11d). The correlation between future change in RMW and precipitation scaling was weakly negative, with $R^2 = 0.08$, and statistically insignificant ($p \geq 0.05$; Figure 11c); however, this was primarily because of Ian as an outlier which had disproportionately low precipitation scaling compared to its future change in RMW. Without this outlier, the correlation would have been strongly negative ($R^2 = 0.49$) and significant. The future decrease in the extent of the inner core in our simulations, together with the findings of Stansfield and Rasmussen (2025)—that as the inner core contracts, convection occurs in a relatively larger portion of the inner core, relative to the inner core's overall area—suggests that the overall area of inner-core convection may increase. No correlation existed between future change in R34 and precipitation scaling ($R^2 \approx 0.00$; figure not shown). However, the correlation between the future change in 700 hPa ω and precipitation scaling was strongly positive ($R^2 = 0.75$) and statistically significant (Figure 11d). This suggests that future changes in RMW and R34 had no significant influence on precipitation scaling, whereas future changes in vertical velocity had a significant and relatively large influence on precipitation scaling. We also calculated the correlation between precipitable water scaling and precipitation scaling (not shown), which was strongly positive ($R^2 = 0.58$) and statistically significant. However, precipitable water scaling explained less of the variance in precipitation scaling than increases in 700 hPa ω did, suggesting that future increases in convection had a greater influence on precipitation scaling than precipitable water scaling had. Increasing future TC intensity has been previously found to influence the rate of precipitation increases (Ruan & Wu, 2018); therefore, we also calculated the linear correlation between future change in peak TC intensity and precipitation scaling. However, the correlation was weakly negative ($R^2 = 0.11$) and statistically insignificant ($p \geq 0.05$), suggesting that future changes in peak TC intensity were not the main drivers for future precipitation increases.

Our earlier result that TC dynamics had a large influence on the super-CC scaling of precipitation is also supported by the horizontal spatial patterns of future changes in 700 hPa vertical motion (Figures 12 and 13). Regions with enhanced (inhibited) precipitation (Figures 8 and 9) tend to coincide with regions where updrafts were enhanced (suppressed), indicating enhanced convection (subsidence). We examined vertical cross-sections of TC-following vertical velocity (figures not shown) and confirmed that 700 hPa is a representative level. When comparing the future changes in 700 hPa vertical velocity (Figures 12 and 13) and in precipitable water scaling (Figures 14 and 15) with future changes in precipitation (Figures 8 and 9) for each of the TCs, we see that the spatial patterns for changes in vertical velocity are more representative of the changes in precipitation than the changes in precipitable water scaling are. This suggests that future changes in the spatial structure of TC precipitation are more associated with future dynamical changes rather than with future changes in water vapor. Statistics in 700 hPa vertical velocity (ω) support this idea: The magnitude of 5th-percentile 700-hPa ω (representing strong convection) increased over land by 6%–42% for all TCs except Harvey (not shown) and increased over ocean by 17%–60% for all TCs. The magnitude of mean 700 hPa ω over land and ocean together increased by 8%–30% for all TCs except for Ian, which produced a 4% decrease. These results demonstrate the importance of enhanced convection in super-CC future precipitation scaling. Furthermore, the correlation between precipitable water scaling and precipitation scaling, along with super-CC precipitable water in some TC cases, suggests that the thermodynamic and dynamic changes may work in concert to enhance precipitation at super-CC rates, with more moisture being lifted by stronger updrafts. In addition to the changes in 700 hPa vertical velocity area-averaged around the TC, the tendency for the greatest wind enhancements to occur within the inner core

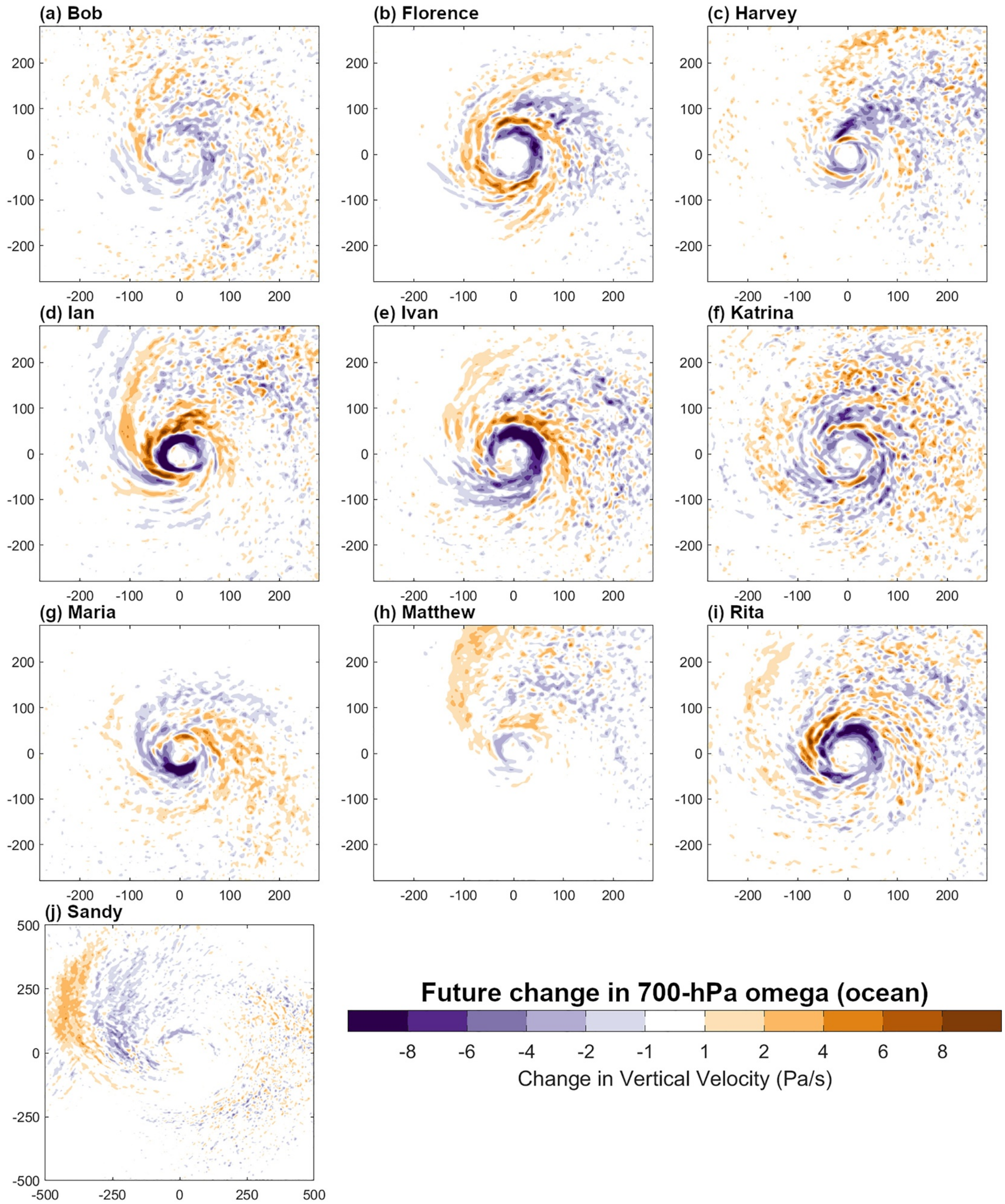

Figure 13. Same as Figure 12, but for when each tropical cyclone is centered over ocean.

(Figure 4) provides additional support, as this indicates the enhancement of the inner core and its convection as a result (Carrasco et al., 2014), despite the presence of less moisture-saturated air at 700 hPa entraining into nine of 10 TCs in the future climate (not shown), though all at varying spatial extents and magnitudes.

4.4. TC Translation Speed

We next considered future changes in TC translation speed as one possible explanation for the regionally averaged precipitation changes, recognizing that future wind perturbations were not applied in our simulations; therefore they do not account for potential future changes in atmospheric circulation and only account for any changes in translation speed due to changes in temperature gradients that can alter wind and TC steering flow. TC translation speeds averaged during the approach to landfall through after landfall ranged between 15 and 45 km/hr in the historical simulations, increasing to 16–49 km/hr in the future simulations (Figure 16a). Compared with the

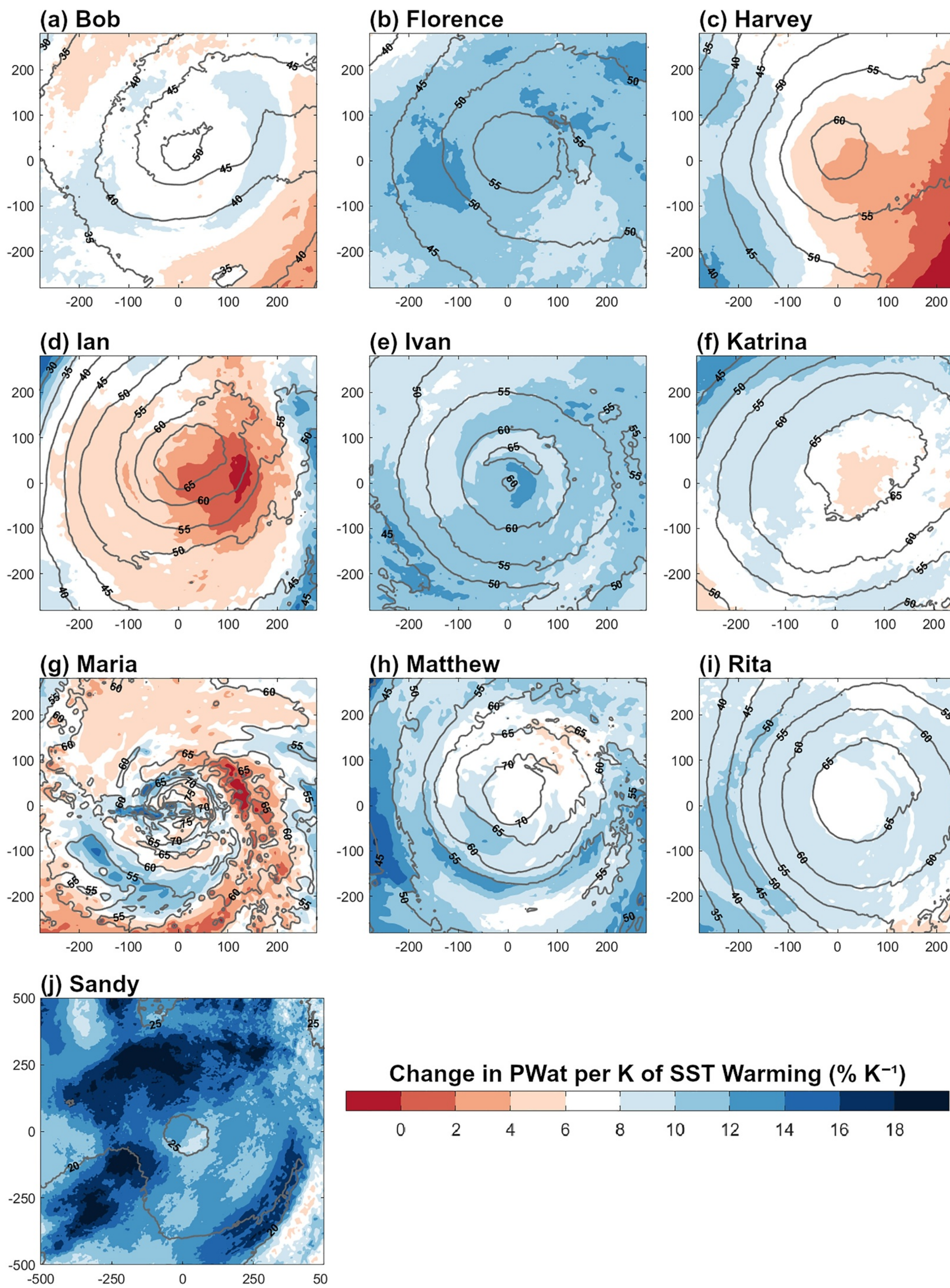

Figure 14. Ensemble-mean future scaling of precipitable water with respect to future increases in SSTs (% K^{-1}) for Hurricanes Bob through Sandy (a–j) while centered over land. Red shading indicates sub-CC scaling of precipitable water, while blue shading indicates super-CC scaling. Gray contours show the historical precipitable water for each tropical cyclone (TC) (mm). The *x* and *y*-axes show the distance away from the TC center (km).

observed translation speed calculated using six-hourly data from HURDAT2, the majority of TCs simulated in the historical climate (six of ten) had a fast bias by up to 54% in translation speed, while the remaining four TCs exhibited slow biases of up to 20% (Figure 16b). TC translation speeds increased for the majority of TCs in the future (Figure 16c). Six of ten TCs increased in translation speed in the future by up to 4 km/hr (3%–14%), while translation speeds decreased for the remaining four TCs with slowdowns of up to 12 km/hr (2%–34%). Our results

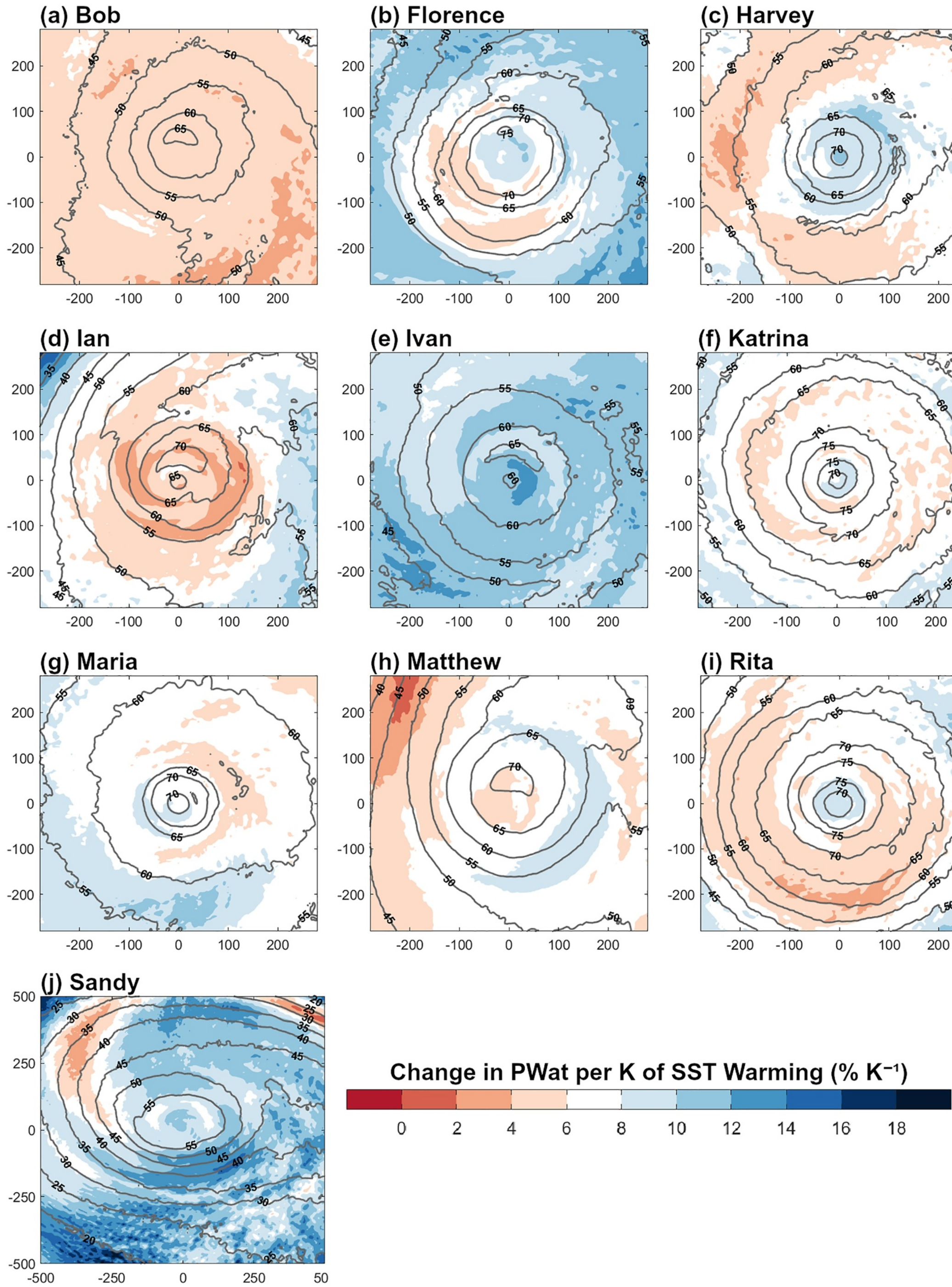

Figure 15. Same as Figure 14, but for when tropical cyclones were centered over ocean.

suggest that the future of TC translation speed changes due to thermodynamics is uncertain, as there is the potential for both speedup and slowdown of TC translation speeds, with the speedups more moderate than the slowdowns. All 10 TCs had a weakly positive ($R^2 = 0.06$) and statistically insignificant ($p \geq 0.05$; Figure 16d) correlation between future changes in translation speed and future changes in area-averaged storm-total precipitation over the land regions impacted by the TC, indicating that future changes in translation speed played a minimal role in enhancing future regional precipitation.

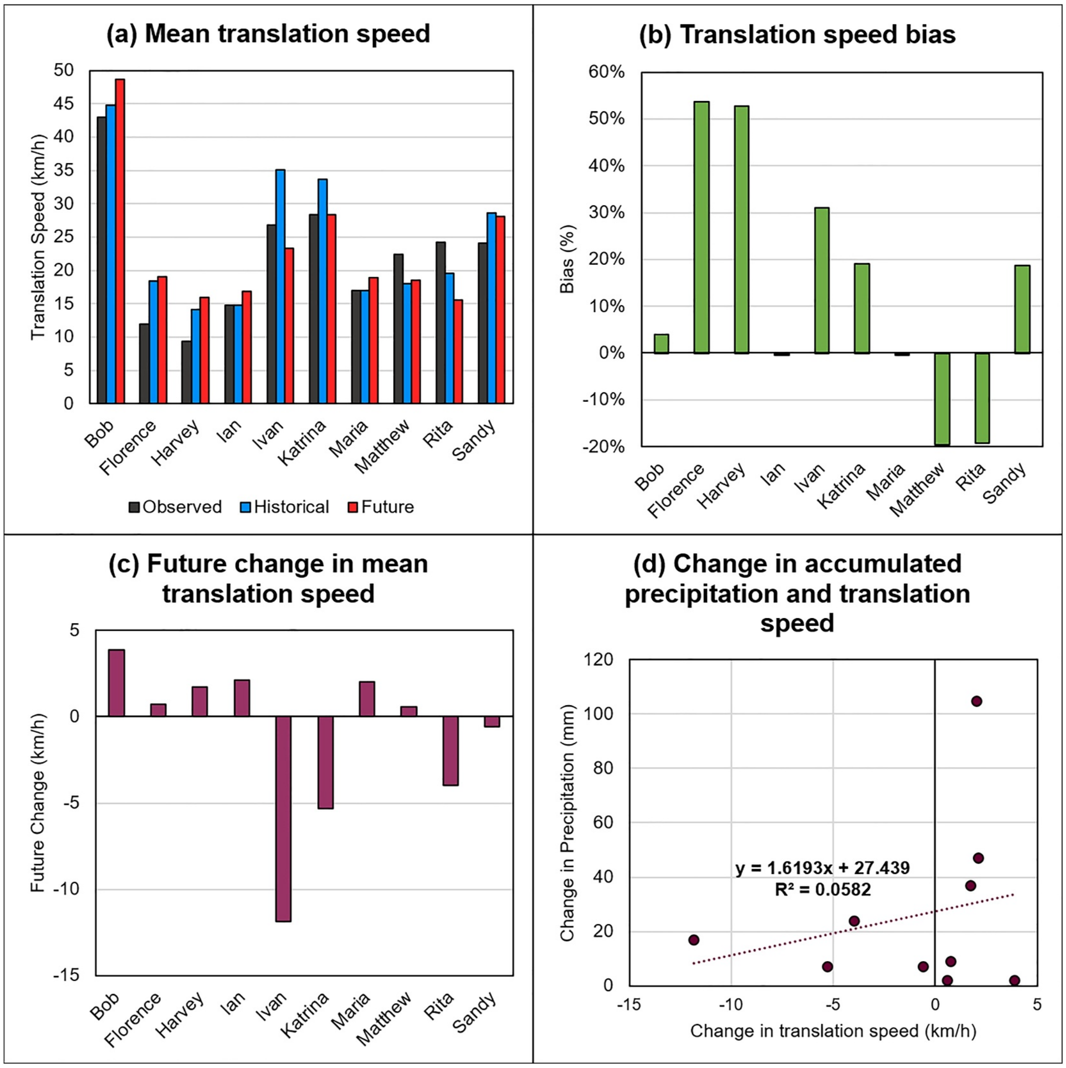

Figure 16. (a) Tropical cyclone (TC) translation speeds (km/h) averaged from approximately 24 hr before landfall (or close approach for TCs that did not make landfall) through the end of the analysis periods (Table 1) from HURDAT2 observations (black) and the ensemble-mean historical (blue) and future (red) simulations. (b) The model bias in translation speed (%), calculated as (ensemble-mean historical simulation minus observations)/observations. (c) The future change in TC translation speed (km/h) calculated as ensemble-mean future simulation minus ensemble-mean future simulation averaged over the same time period as in (a). (d) Scatterplot of the relationship between future change in TC translation speed (km/h) on the x-axis (from (a)) and future changes in land-based regionally averaged precipitation (mm) on the y-axis (from Figure 6d). The points indicate the ensemble mean for each TC, while the dashed line represents the linear trendline for the data points.

5. Discussion and Conclusions

The purpose of this study was two-fold: (a) to project future changes in Atlantic TC precipitation during the mid-21st century under a high-emissions scenario and (b) to evaluate how future TC precipitation scaling compares to the theoretical CC rate and understand the physical mechanisms behind any deviations from CC. Using convection-permitting pseudo-global warming simulations of ten historically impactful Atlantic TC events, we found that future storm-total precipitation increased up to ∼1.5 times the historical. These results are consistent with other studies (Carroll-Smith et al., 2021; Knutson et al., 2013, 2015; Patricola & Wehner, 2018), though many studies project similar precipitation increases for the late-21st century. Future precipitation over land increased by at least 14% for eight of ten TCs in a TC-following framework, indicating greater future impacts from TC precipitation. Future TC precipitation rates tended to increase within the TC inner core, while precipitation decreased in portions of the outer rainbands for many of the TCs, suggesting that inner-core precipitation may pose a greater threat in the future climate.

We also found that nine of ten TCs exhibited super-CC precipitation scaling of up to 17% K^{-1} or nearly 2.5 times that of CC. This shows that TC precipitation may increase beyond simple thermodynamic estimates, suggesting that the CC relationship is not a reliable benchmark for projecting future TC precipitation. Furthermore, we found that future precipitable water scaled at lower rates than precipitation did for nine of ten TCs, suggesting that thermodynamic changes alone cannot explain the projected super-CC increases in precipitation. We analyzed future changes in vertical motion and TC size and their relationships with future precipitation scaling to identify potential mechanisms for super-CC scaling. We found strong evidence that future changes in vertical motion support super-CC TC precipitation scaling. In particular, regions of the TCs with enhanced (inhibited) updrafts corresponded to regions of enhanced (suppressed) precipitation. In addition, future TC precipitation scaling and vertical velocity changes were strongly and significantly correlated. This shows that enhanced convection, together with enhanced precipitable water (which had future scaling that was also strongly and significantly correlated with precipitation scaling), likely acted in concert to enhance future TC precipitation at super-CC rates, potentially with an expansion of areas of convection in the inner core to move greater quantities of water vapor upward at faster speeds (Stansfield & Rasmussen, 2025). Future changes in precipitation, however, may be affected by any future changes in frictional convergence, tropospheric wind shear, and interactions with baroclinic features (Lu et al., 2018), with frictional convergence dependent on boundary layer conditions and TC-surface interactions, while tropospheric wind shear would be dependent on synoptic conditions and the presence of baroclinic features near TCs that may be situational. There is also the potential for additional precipitation enhancement due to future changes in land cover as was found for Hurricane Harvey (Zhang et al., 2018), though our study does not account for this.

In terms of TC-size, future RMW contracted in 9 of the 10 TCs, while results were inconclusive for R34. This suggests that the inner core may contract inward in future TCs, potentially enhancing convection. Despite the significant future changes in RMW, however, the relationship between changes in RMW and precipitation scaling was weak and insignificant due to an outlier (Ian), which had disproportionately low future precipitation scaling relative to its future increase in convection. This was likely due to substantial dry-air entrainment into Ian as indicated by future changes in 700 hPa RH and the sub-CC scaling of precipitable water. This suggests that in cases of extensive dry-air entrainment, enhanced convection alone is not enough to support super-CC increases in TC precipitation if atmospheric moisture content is insufficient.

Future changes in regional storm-total TC precipitation and TC translation speeds appeared unrelated to each other, as their correlation was weak and statistically insignificant. The former may have been influenced by cases in which sensitivity to TC track deviations was high. This suggests that future changes in TC translation speed may not have as consistent of a role in future TC precipitation impacts as changes in convection may have.

In summary, Atlantic TC precipitation may increase up to 1.5 times the historical by the mid-21st century, scaling at nearly 2.5 times CC. This is due to both enhanced atmospheric moisture and enhanced convection. These results suggest that future landfalling TC precipitation will have a greater impact throughout 2040–2060, regardless of future changes in TC translation speed or TC size, increasing the chance of fatalities and property damage from freshwater flooding. Given that our simulations were performed for the mid-21st century under a high-emissions scenario, it is important to acknowledge that our results depend on the high equilibrium climate sensitivity of E3SM v1.1 (Golaz et al., 2022). Therefore, it is possible that the level of warming projected by E3SM v1.1 for the mid-21st century may happen at a later time. In addition, it is possible that future greenhouse gas emissions may follow a different trajectory than SSP585, which would also likely lead to the changes projected in this study to occur later than the mid-21st century. Additional uncertainty came from the usage of a single microphysics scheme and planetary boundary layer scheme as TCs are sensitive to changes in nucleation types represented in microphysics schemes (Wu et al., 2021) and how the boundary layer is represented (Wang & Ming, 2020). Potential sensitivity to microphysics and planetary boundary layer schemes would be valuable to investigate in future studies, as supercomputing resource limitations led us to prioritize conducting ensembles of simulations for 10 TC events.

As our simulations used prescribed future climate conditions based on one global climate model, more research should be conducted projecting future changes in TC precipitation in the mid-21st century using other global climate models for comparison. Research using hydrologic and storm surge models should also be conducted to determine how the magnitude of flooding would increase under the future TC precipitation projections from this study. Finally, we recognize that the simulations used in this study are from an atmosphere-only model with prescribed SST, which may introduce uncertainty into the future projections, given the importance of atmosphere-ocean interactions for future TC precipitation projections in simulations from global climate models (Huang et al., 2021) and nonconvection-permitting regional models (Danso et al., 2024). We plan to investigate this in future work using convection-permitting simulations that minimize the SST biases typical of global climate models (Richter, 2015; Zuidema et al., 2016) that can have substantial impacts on simulated TCs (Hsu et al., 2019).

Data Availability Statement

Data and software are available at the following:

- Atlantic Hurricane Database (HURDAT2): Landsea and Franklin (2013).
- WRF v4.3.0 source code: Skamarock et al. (2021).
- WRF namelist files from the simulations: Forbis (2025).
- The ERA5 reanalysis: Hersbach et al. (2020).
- E3SM v1.1 model outputs: Bader et al. (2019, 2020).
- SSP 5–8.5 greenhouse gas concentrations: Meinshausen et al. (2020).
- 4-km Gridded Data Stage IV Data: Du (2011).
- Integrated Multi-satellite Retrievals for Global Precipitation Measurement: Huffman et al. (2020).
- GridMET precipitation data: Abatzoglou (2013).

Acknowledgments

This research was supported by the U.S. Department of Energy, Office of Science, Office of Biological and Environmental Research, Earth and Environmental Systems Modeling Program, under Early Career Research Program Award Number DE-SC0021109. This work used the Extreme Science and Engineering Discovery Environment (XSEDE) computing resource Stampede2 and Ranch, which is supported by National Science Foundation Grant ACI-1548562, through allocations ATM190012 and ATM190016. This work used Stampede2 and Ranch at the Texas Advanced Computing Center at The University of Texas at Austin through allocation EES230023 from the Advanced Cyberinfrastructure Coordination Ecosystem: Services & Support (ACCESS) program (Boerner et al., 2023), which is supported by U.S. National Science Foundation Grants 2138259, 2138286, 2138307, 2137603, and 2138296. The authors acknowledge the Texas Advanced Computing Center (TACC) at The University of Texas at Austin for providing HPC resources that have contributed to the research results reported within this paper. URL: http://www.tacc.utexas.edu. The data were provided by the research data archive (RDA) of the Computational and Information Systems Laboratory at the National Center for Atmospheric Research. NCAR is supported by Grants from the National Science Foundation. Data were obtained from the Energy Exascale Earth System Model project, sponsored by the U.S. Department of Energy, Office of Science, and Office of Biological and Environmental Research. This research was supported as part of the Energy Exascale Earth System Model (E3SM) project, funded by the U.S. Department of Energy, Office of Science and Office of Biological and Environmental Research. We thank three anonymous reviewers for their constructive comments that helped improve the manuscript.

References

Abatzoglou, J. T. (2013). Development of gridded surface meteorological data for ecological applications and modelling [Dataset]. *International Journal of Climatology*, *33*(1), 121–131. https://doi.org/10.1002/joc.3413

Bader, D. C., Leung, R., Taylor, M., & McCoy, R. B. (2019). E3SM-Project E3SM1.1 model output prepared for CMIP6 CMIP historical Version 20220407 [Dataset]. *Earth System Grid Federation*. https://doi.org/10.22033/ESGF/CMIP6.11485

Bader, D. C., Leung, R., Taylor, M., & McCoy, R. B. (2020). E3SM-Project E3SM1.1 model output prepared for CMIP6 ScenarioMIP ssp585 Version 20220407 [Dataset]. *Earth System Grid Federation*. https://doi.org/10.22033/ESGF/CMIP6.15179

Berner, J., Ha, S.-Y., Hacker, J. P., Fournier, A., & Snyder, C. (2011). Model uncertainty in a mesoscale ensemble prediction system: Stochastic versus multiphysics representations. *Monthly Weather Review*, *139*(6), 1972–1995. https://doi.org/10.1175/2010MWR3595.1

Boerner, T. J., Deems, S., Furlani, T. R., Knuth, S. L., & Towns, J. (2023). ACCESS: Advancing innovation: NSF's advanced cyberinfrastructure coordination Ecosystem: Services & support. In *Practice and experience in advanced research computing (PEARC '23), July 23–27, 2023*, ACM, 4. https://doi.org/10.1145/3569951.3597559

Brennan, M., Brown, D., & Pope, L. (2023). Recent trends in tropical cyclone fatalities in the United States. Retrieved from https://blog.ametsoc.org/2023/08/08/recent-trends-in-tropical-cyclone-fatalities-in-the-united-states/

Carrasco, C. A., Landsea, C. W., & Lin, Y.-L. (2014). The influence of tropical cyclone size on its intensification. *Weather and Forecasting*, *29*(3), 582–590. https://doi.org/10.1175/WAF-D-13-00092.1

Carroll-Smith, D., Trapp, R. J., & Done, J. M. (2021). Exploring inland tropical cyclone rainfall and tornadoes under future climate conditions through a case study of hurricane ivan. *Journal of Applied Meteorology and Climatology*, *60*(1), 103–118. https://doi.org/10.1175/JAMC-D-20-0090.1

Chavas, D. R., Knaff, J. A., & Klotzbach, P. (2024). A simple model for predicting tropical cyclone minimum central pressure from intensity and size. *Weather and Forecasting*, *40*(2), 333–346. in press. https://doi.org/10.1175/WAF-D-24-0031.1

Chen, F., & Dudhia, J. (2001). Coupling an advanced land surface-hydrology model with the Penn State–NCARMM5 modeling system. Part I: Model implementation and sensitivity. *Monthly Weather Review*, *129*(4), 569–585. https://doi.org/10.1175/1520-0493(2001)129,0569:CAALSH.2.0.CO;2

Danso, D. K., Patricola, C. M., Kurian, J., Chang, P., Klotzbach, P., & Lin, I.-I. (2024). Air-sea coupling influence on projected changes in major Atlantic hurricane events. *Weather and Climate Extremes*, *43*, 100649. https://doi.org/10.1016/j.wace.2024.100649

Dinan, T. (2017). Projected increases in hurricane damage in the United States: The role of climate change and coastal development. *Ecological Economics*, *138*, 186–198. https://doi.org/10.1016/j.ecolecon.2017.03.034

Dougherty, E., & Rasmussen, K. L. (2021). Variations in flash flood-producing storm characteristics associated with changes in vertical velocity in a future climate in the Mississippi river basin. *Journal of Hydrometeorology*, *22*(3), 671–687. https://doi.org/10.1175/JHM-D-20-0254.1

Du, J. (2011). NCEP/EMC 4KM gridded data (GRIB) stage IV data version 1.0 [Dataset]. *UCAR/NCAR - Earth Observing Laboratory*. https://doi.org/10.5065/D6PG1QDD

Duda, J. D., Wang, X., Kong, F., Xue, M., & Berner, J. (2016). Impact of a stochastic kinetic energy backscatter scheme on warm season convection-allowing ensemble Forecasts. *Monthly Weather Review*, *144*(5), 1887–1908. https://doi.org/10.1175/MWR-D-15-0092.1

European Centre for Medium-Range Weather Forecasts. (2017). ERA5 reanalysis. *Research Data Archive at the National Center for Atmospheric Research, Computational and Information Systems Laboratory*. updated monthly. https://doi.org/10.5065/D6X34W69. Accessed 9 Feb 2022.

Forbis, D. C. (2025). Forbis and Patricola 2025 WRF namelists. *GitHub*. [Collection] https://github.com/DakFor/Forbis_and_Patricola_2025_WRF_Namelists/releases/tag/v1.0

Forbis, D. C., Patricola, C. M., Bercos-Hickey, E., & Gallus, W. A., Jr. (2024). Mid-century climate change impacts on tornado-producing tropical cyclones. *Weather and Climate Extremes*, *44*, 1–14. https://doi.org/10.1016/j.wace.2024.100684

Frisius, T. (2015). What controls the size of a tropical cyclone? Investigations with an axisymmetric model. *Quarterly Journal of the Royal Meteorological Society*, *141*(691), 2457–2470. https://doi.org/10.1002/qj.2537

Golaz, J.-C., Van Roekel, L. P., Zheng, X., Roberts, A. F., Wolfe, J. D., Lin, W., et al. (2022). The DOE E3SM model version 2: Overview of the physical model and initial model evaluation. *Journal of Advances in Modeling Earth Systems*, *14*(12), 1–51. https://doi.org/10.1029/2022MS003156

Gori, A., Lin, N., Xi, D., & Emanuel, K. (2022). Tropical cyclone climatology change greatly exacerbates US extreme rainfall-surge hazard. *Nature Climate Change*, *12*(2), 171–178. https://doi.org/10.1038/s41558-021-01272-7

Hersbach, H., Bell, B., Berrisford, P., Hirahara, S., Horányi, A., Muñoz-Sabater, J., et al. (2020). The ERA5 global reanalysis [Dataset]. *Quarterly Journal of the Royal Meteorological Society*, *146*(730), 1999–2049. https://doi.org/10.1002/qj.3803

Hill, K. A., & Lackmann, G. M. (2009). Influence of environmental humidity on tropical cyclone size. *Monthly Weather Review*, *137*(10), 3294–3315. https://doi.org/10.1175/2009MWR2679.1

Hsu, W.-C., Patricola, C. M., & Chang, P. (2019). The impact of climate model sea surface temperature biases on tropical cyclone simulations. *Climate Dynamics*, *53*(1), 173–192. https://doi.org/10.1007/s00382-018-4577-5

Huang, H., Patricola, C. M., & Collins, W. D. (2021). The influence of ocean coupling on simulated and projected tropical cyclone precipitation in the HighResMIP–PRIMAVERA simulations. *Geophysical Research Letters*, *48*(20), e2021GL094801. https://doi.org/10.1029/2021gl094801

Huffman, G. J., Bolvin, D. T., Braithwaite, D., Hsu, K. L., Joyce, R. J., Kidd, C., et al. (2020). Integrated multi-satellite Retrievals for the global precipitation measurement (GPM) mission (IMERG) [Dataset]. In *Satellite precipitation measurement* V. Levizzani, C. Kidd, D. B. Kirschbaum, C. D. Kummerow, K. Nakamura, & F. J. Turk (Eds.), Vol. *67*, 343–353. *Advances in global change research*. https://doi.org/10.1007/978-3-030-24568-9_19. Springer

Iacono, M. J., Delamere, J. S., Mlawer, E. J., Shephard, M. W., Clough, S. A., & Collins, W. D. (2008). Radiative forcing by long-lived greenhouse gases: Calculations with the AER radiative transfer models. *Journal of Geophysical Research*, *113*, D13. https://doi.org/10.1029/2008JD009944

Janjić, Z. I. (1994). The step-mountain eta coordinate model: Further developments of the convection, viscous sublayer, and turbulence closure schemes. *Monthly Weather Review*, *122*(5), 927–945. https://doi.org/10.1175/1520-0493(1994)122,0927:TSMECM.2.0.CO;2

Kim, H.-S., Vecchi, G. A., Knutson, T. R., Anderson, W. G., Delworth, T. L., Rosati, A., et al. (2014). Tropical cyclone simulation and response to CO_2 doubling in the GFDL CM2.5 high-resolution coupled climate model. *Journal of Climate*, *27*(21), 8034–8054. https://doi.org/10.1175/JCLI-D-13-00475.1

Knutson, T. R., Sirutis, J. J., Vecchi, G. A., Garner, S., Zhao, M., Kim, H.-S., et al. (2013). Dynamical downscaling projections of twenty-first-century atlantic hurricane activity: CMIP3 and CMIP5 model-based scenarios. *Journal of Climate*, *26*(17), 6591–6617. https://doi.org/10.1175/JCLI-D-12-00539.1

Knutson, T. R., Sirutis, J. J., Zhao, M., Tuleya, R. E., Bender, M., Vecchi, G. A., et al. (2015). Global projections of intense tropical cyclone activity for the late twenty-first century from dynamical downscaling of CMIP5/RCP4.5 scenarios. *Journal of Climate*, *28*(18), 7203–7224. https://doi.org/10.1175/JCLI-D-15-0129.1

Konrad, C. E., II, Meaux, M. F., & Meaux, D. A. (2002). Relationships between tropical cyclone attributes and precipitation totals: Considerations of scale. *International Journal of Climatology*, *22*(2), 237–247. https://doi.org/10.1002/joc.721

Kossin, J. P. (2018). A global slowdown of tropical-cyclone translation speed. *Nature*, *558*(7708), 104–107. https://doi.org/10.1038/s41586-018-0158-3

Landsea, C. W., & Franklin, J. L. (2013). Atlantic hurricane Database uncertainty and presentation of a new Database format [Dataset]. *Monthly Weather Review*, *141*(10), 3576–3592. https://doi.org/10.1175/mwr-d-12-00254.1

Lenderink, G., Barbero, R., Loriaux, J. M., & Fowler, H. J. (2017). Super-clausius–clapeyron scaling of extreme hourly convective precipitation and its relation to large-scale atmospheric conditions. *Journal of Climate*, *30*(15), 6037–6052. https://doi.org/10.1175/JCLI-D-16-0808.1

Liu, M., Vecchi, G. A., Smith, J. A., & Knutson, T. R. (2019). Causes of large projected increases in hurricane precipitation rates with global warming. *Npj Clim. And Atmospheric Sci.*, *2*, 1–5. https://doi.org/10.1038/s41612-019-0095-3

Lu, P., Lin, N., Emanuel, K., Chavas, D., & Smith, J. (2018). Assessing hurricane rainfall mechnisms using a physics-based model: Hurricanes isabel (2003) and Irene (2011). *Journal of the Atmospheric Sciences*, *75*(7), 2337–2358. https://doi.org/10.1175/JAS-D-17-0264.1

Matyas, C. J. (2010). Associations between the size of hurricane rain fields at landfall and their surrounding environments. *Meteorology and Atmospheric Physics*, *106*(3–4), 135–148. https://doi.org/10.1007/s00703-009-0056-1

Meinshausen, M., Nicholls, Z. R. J., Lewis, J., Gidden, M. J., Vogel, E., Freund, M., et al. (2020). The shared socio-economic pathway (SSP) greenhouse gas concentrations and their extensions to 2500 [Dataset]. *Geoscientific Model Development*, *13*(8), 3571–3605. https://doi.org/10.5194/gmd-13-3571-2020

Mendelsohn, R., Emanuel, K., Chonabayashi, S., & Bakkensen, L. (2012). The impact of climate change on global tropical cyclone damage. *Nature Clim. Communications*, *2*(3), 205–209. https://doi.org/10.1038/nclimate1357

Nekkali, Y. S., Osuri, K. K., & Das, A. K. (2022). Numerical modeling of tropical cyclone size over the bay of Bengal: Influence of microphysical processes and horizontal resolution. *Meteorology and Atmospheric Physics*, *134*(4), 72. https://doi.org/10.1007/s00703-022-00915-4

NOAA National Centers for Environmental Information (NCEI). (2024). U.S. 2024 billion-dollar weather and climate disasters. https://doi.org/10.25921/stkw-7w73

Patricola, C. M., & Wehner, M. F. (2018). Anthropogenic influences on major tropical cyclone events. *Nature*, *563*(7731), 339–346. https://doi.org/10.1038/s41586-018-0673-2

Rappaport, E. N. (2014). Fatalities in the United States from Atlantic tropical cyclones: New data and interpretation. *Bulletin of the American Meteorological Society*, *95*(3), 341–346. https://doi.org/10.1175/BAMS-D-12-00074.1

Reed, K. A., Stansfield, A. M., Wehner, M. F., & Zarzycki, C. M. (2020). Forecasted attribution of the human influence on hurricane florence. *Science Advances*, *6*, 1–8. https://doi.org/10.1126/sciadv.aaw9253

Reed, K. A., Wehner, M. F., & Zarzycki, C. M. (2022). Attribution of 2020 hurricane season extreme rainfall to human-induced climate change. *Nature Communications*, *13*, 1–6. https://doi.org/10.1038/s41467-022-29379-1

Richter, I. (2015). Climate model biases in the eastern tropical oceans: Causes, impacts and ways forward. *Wiley Interdisciplinary Reviews: Climate Change*, *6*(3), 345–358. https://doi.org/10.1002/wcc.338

Risser, M. D., & Wehner, M. F. (2017). Attributable human-induced changes in the likelihood and magnitude of the observed extreme precipitation during hurricane Harvey. *Geophysical Research Letters*, *44*(24), 12457–12464. https://doi.org/10.1002/2017GL075888

Ruan, Z., & Wu, Q. (2018). Precipitation, convective clouds, and their connections with tropical cyclone intensity and intensity change. *Geophysical Research Letters*, *45*(2), 1098–1105. https://doi.org/10.1002/2017GL076611

Schär, C., Frei, C., Lüthi, D., & Davies, H. C. (1996). Surrogate climate-change scenarios for regional climate models. *Geophysical Research Letters*, *23*(6), 669–672. https://doi.org/10.1029/96GL00265

Schenkel, B. A., Noble, C., Chavas, D., Chan, K. T. F., Barlow, S. J., Singh, A., & Musgrave, K. (2023). Recent progress in research and forecasting of tropical cyclone outer size. *Tropical Cyclone Research and Review*, *12*(3), 151–164. https://doi.org/10.1016/j.tcrr.2023.09.002

Scoccimarro, E., Gualdi, S., Villarini, G., Vecchi, G. A., Zhao, M., Walsh, K., & Navarra, A. (2014). Intense precipitation events associated with landfalling tropical cyclones in response to a warmer climate and increased CO_2. *Journal of Climate*, *27*(12), 4642–4654. https://doi.org/10.1175/JCLI-D-14-00065.1

Sena, A. C. T., Patricola, C. M., Camargo, S. J., & Sobel, A. H. (2024). The atmospheric effect of aerosols on future tropical cyclone frequency and precipitation in the energy Exascale Earth system model. *Climate Dynamics*, *2024*(9), 8755–8788. https://doi.org/10.1007/s00382-024-07359-z

Shutts, G. (2005). A kinetic energy backscatter algorithm for use in ensemble prediction systems. *Quarterly Journal of the Royal Meteorological Society*, *131*(612), 3079–3102. https://doi.org/10.1256/qj.04.106

Skamarock, W. C., Klemp, J. B., Dudhia, J., Gill, D. O., Liu, Z., Berner, J., et al. (2021). A description of the advanced research WRF version 4.3 [Software]. *NCAR Tech. Note NCAR/TN-556+STR*, 145. https://doi.org/10.5065/1dfh-6p97

Stansfield, A. M., & Rasmussen, K. L. (2025). The response of tropical cyclone inner core and outer core rainband precipitation to warming in idealized convection-permitting WRF. *Journal of Geophysical Research: Atmospheres*, *130*(4), e2024JD042217. https://doi.org/10.1029/2024JD042217

Stansfield, A. M., & Reed, K. A. (2021). Tropical cyclone precipitation response to surface warming in aquaplanet simulations with uniform thermal forcing. *JGR Atmospheres*, *126*(24), 1–18. https://doi.org/10.1029/2021JD035197

Stansfield, A. M., & Reed, K. A. (2023). Global tropical cyclone precipitation scaling with sea surface temperature. *npj Climate and Atmospheric Science*, *6*(1), 60. https://doi.org/10.1038/s41612-023-00391-6

Tebaldi, C., Straussss, B. H., & Zervas, C. E. (2012). Modelling sea level rise impacts on storm surges along US coasts. *Environmental Research Letters*, *7*(1), 014032. https://doi.org/10.1088/1748-9326/7/1/014032

Thompson, G., Field, P. R., Rasmussen, R. M., & Hall, W. D. (2008). Explicit Forecasts of winter precipitation using an improved bulk microphysics scheme. Part II: Implementation of a new snow parameterization. *Monthly Weather Review*, *136*(12), 5095–5115. https://doi.org/10.1175/2008MWR2387.1

Touma, D., Stevenson, S., Camargo, S. J., Horton, D. E., & Diffenbaugh, N. S. (2019). Variations in the intensity and spatial extent of tropical cyclone precipitation. *Geophysical Research Letters*, *46*(23), 13992–14002. https://doi.org/10.1029/2019GL083452

Trenberth, K. E., Dai, A., Rasmussen, R. M., & Parsons, D. B. (2003). The changing character of precipitation. *Bulletin of the American Meteorological Society*, *84*(9), 1205–1218. https://doi.org/10.1175/BAMS-84-9-1205

Tu, S., Chan, J. C. L., Xu, J., Zhong, Q., Zhou, W., & Zhang, Y. (2022). Increase in tropical cyclone rain rate with translation speed. *Nature Communications*, *13*(1), 7325. https://doi.org/10.1038/s41467-022-35113-8

Villarini, G., Lavers, D. A., Scoccimarro, E., Zhao, M., Wehner, M. F., Vecchi, G. A., et al. (2014). Sensitivity of tropical cyclone rainfall to idealized global-scale forcings. *Journal of Climate*, *27*(12), 4622–4641. https://doi.org/10.1175/JCLI-D-13-00780.1

Wang, C.-X., & Ming, Y. (2020). The uncertainty of tropical cyclone intensity and structure based on different paramterization schemes of planetary boundary layer. *Journal of Tropical Meteorology*, *26*(3), 377–389. https://doi.org/10.46267/j.1006-8775.2020.033

Wu, D., Zhang, F., Chen, X., Ryzhkov, A., Zhao, K., Kumjian, M. R., et al. (2021). Evaluation of microphysics schemes in tropical cyclones using polarimeteric radar observations: Convective precipitation in an outer rainband. *Monthly Weather Review*, *149*(4), 1055–1068. https://doi.org/10.1175/MWR-D-19-0378.1

Yamaguchi, M., Chan, J. C. L., Moon, I.-J., Yoshida, K., & Mizuta, R. (2020). Global warming changes tropical cyclone translation speed. *Nature Communications*, *11*, 1–7. https://doi.org/10.1038/s41467-019-13902-y

Zhang, W., Villarini, G., Vecchi, G. A., & Smith, J. A. (2018). Urbanization exacerbated the rainfall and flooding caused by hurricane Harvey in houston. *Nature*, *563*(7731), 384–388. https://doi.org/10.1038/s41586-018-0676-z

Zuidema, P., Chang, P., Medeiros, B., Kirtman, B. P., Mechoso, R., Schneider, E. K., et al. (2016). Challenges and prospects for reducing coupled climate model SST biases in the eastern tropical Atlantic and Pacific oceans: The US CLIVAR Eastern Tropical Oceans Synthesis Working Group. *Bulletin of the American Meteorological Society*, *97*(12), 2305–2328. https://doi.org/10.1175/bams-d-15-00274.1